# Current State of $Ga_2O_3$-Based Electronic and Optoelectronic Devices. Brief Review

## A. A. Petrenko[1], Ya. N. Kovach[1], D. A. Bauman[1], M. A. Odnoblyudov[1,2], V. E. Bougrov[1] and A. E. Romanov[1,3]

[1]Institute of Advanced Data Transfer Systems, ITMO University, Kronverksky Pr. 49, bldg. A, St. Petersburg, 197101, Russia
[2]Peter the Great St. Petersburg Polytechnic University, Polytechnicheskaya 29, St. Petersburg, 195251, Russia
[3]Ioffe Physical-Technical Institute, Russian Academy of Sciences, Polytechnicheskaya 26, St. Petersburg, 194021, Russia

**Abstract.** In this review, we consider the main gallium oxide areas of application in electronics and optoelectronics with focus on power electronics devices (rectifiers, field effect transistors), solar-blind photodetectors, luminescent devices, gas sensors, spintronic and memory devices. As an introduction, we provide the valuable data on the basic physical properties of the existing $Ga_2O_3$ polymorphic modifications. We discuss device design based on various gallium oxide crystalline forms including those exploring $Ga_2O_3$ single crystals, thick layers, thin films, nanostructures, and $Ga_2O_3$-based heterostructures. Then, the information on the parameters and characteristics of electronic and optoelectronic devices based on gallium oxide is presented. In addition, recently emerging and requiring additional research $Ga_2O_3$ application fields such as photocatalysis and thermomechanical actuating, are briefly addressed.

## 1. INTRODUCTION

At the moment, in the practice of optoelectronic devices design, a great number of problems are being solved related to improving their characteristics, weight and dimensions, creating new energy-efficient light-emitting and photovoltaic devices such as light emitting diodes (LEDs), laser diodes (LDs), photodetectors, gas sensors, and memory devices. To create optoelectronic devices for different purposes, a variety of semiconductor materials with band gaps are traditionally used: from narrow-gap semiconductors like InSb (0.17 eV), InAs (0.36 eV), Ge (0.67 eV) with semiconductors with bandgaps near Si (1.12 eV) – InP (1.35 eV), GaAs (1.4 eV) to wide band gap SiC (3.2 eV), GaN (3.4 eV) and ultra wide band gap $Ga_2O_3$ (4.9 eV), diamond (5.47 eV), AlN (6.28 eV) [1]. In recent years, ultra wide band gap semiconductors (a band gap of more than 4 eV) are especially in demand, because of their potential advantage to increase the operating temperature range, breakdown voltage and radiation resistance. Also the new opportunity of creating ultraviolet and visible spectral range light-emitting and photosensitive devices emerged. Among all ultra wide band gap semiconductors, the most interesting is gallium oxide, which exists in 6 known polymorphic modifications (α, β, γ, δ, ε, and κ) [2,3]. Each of the gallium oxide polymorphs has its own unique properties and may be utilized as a material for the various devices manufacturing. In this review, the main attention is paid to the prospects for the application of gallium oxide in the field of optoelectronic devices manufacturing.

## 2. BASIC PROPERTIES OF $Ga_2O_3$

Currently 6 gallium oxide phases mentioned above have been described theoretically and experimentally [4–6]. The most popular of all is monoclinic β-$Ga_2O_3$, because it is stable under normal conditions and can remain stable up to a temperature of 1800 °C [7]. The results of

---

Corresponding author: A.A. Petrenko, e-mail: aapetrenko@itmo.ru

studying the dielectric constant of β-Ga$_2$O$_3$ in planes (100), (010), and (001) are known. The experiment measured values from 25 to 450 K and obtained values for room temperature $10.2 \pm 0.2$, $10.87 \pm 0.08$, and $12.4 \pm 0.4$, respectively. A comparative table of theoretical and experimental values of the dielectric constant is presented in ref. [8]. Unique characteristics combination of wide band gap (4.6-4.9 eV) [9], mobility (170 cm$^2$/V·s) [10], breakdown field strength (8 MV/cm) [11] makes β-Ga$_2$O$_3$ extremely interesting material in power electronics applications.

The research results indicate the possibility of obtaining other polymorphs from gallium beta-oxide with increasing pressure and temperature. So, in ref. [12] it is shown that monoclinic α-Ga$_2$O$_3$ can be converted to trigonal β-Ga$_2$O$_3$ under cold compression at a pressure of 19.2 GPa. Moreover, such a phase transition is irreversible, and α-Ga$_2$O$_3$ itself is the only stable phase of gallium oxide in the high-pressure region [13].

By merging the semiconducting and magnetic properties of α-Ga$_2$O$_3$ with metals, a promising spintronic materials were obtained. Thus, Kaneko *et al.* investigated the magnetization hysteresis of α-(Ga$_{1-x}$Fe$_x$)$_2$O$_3$ above room temperature [14]. An additional advantage of α-Ga$_2$O$_3$ is the crystal structure of corundum, similar to sapphire, which makes it possible to improve the quality of the grown epitaxial layers.

Defective cubic spinel-type γ-Ga$_2$O$_3$ previously grown by various methods on sapphire substrates are also of interest for utilization in spintronics, since they demonstrate ferromagnetism at room temperatures being Mn-doped [15].

Hexagonal ε-Ga$_2$O$_3$ has a band gap of about 4.9 eV (calculated using a direct band gap fitting formula) [16], which is comparable to the band gap of the well-known GaN and SiC [17]. Various authors have shown ferroelectric [18] and pyroelectric properties of the epsilon phase, as well as large spontaneous polarization [19].

The growing interest in the use of gallium oxide in semiconductor devices is associated with a number of its characteristic features, which include: large bandgap (from 4.6 to 4.9 eV depending on the phase), high critical electric field strength (8 MV/cm [13], which is comparable to the results for a much more expensive diamond), the radiation [20], chemical and thermal resistance [9]. Gallium oxide has been identified as a potential material for working with high-power electric fields, despite the fact that the operating frequency of the devices is currently limited to 1 GHz [21]. It is often mentioned the existence of not 6, but 4 gallium oxide polymorphs, combining ε-, δ- and κ-phase into one group, since the ε-phase probably imitates the κ-phase due to the rotat-

ing grains formed on the sapphire, cubic δ-phase are traditionally considering as a mixture of the β- and ε- phases [22].

Detailed description of various polymorphs characteristics, as well as the technologies for their preparation are presented in the reviews [9,21,22].

## 3. GAS SENSORS

Gallium oxide attracted much attention in extensively advancing applications in detector systems such as gas sensors. Previously experimentally reported results of detecting wide range of gases utilizing gallium oxide based devices: oxygen, hydrogen, carbon monoxide, nitrogen dioxide, triethylamine, hydrogen sulfide, sulfur dioxide, ammonia.

There are references to several fundamental approaches to the creation of various oxygen detectors based on Ga$_2$O$_3$. The annealing of the gallium oxide film [23] transform the grain size and surface quality, which leads to a change in the O$_2$ detection properties. So, at a higher temperature and duration of annealing, the response time decreases. Bartic *et al.* in ref. [24] also showed that the sensitivity of the detector does not depend on the pad types. Ogita *et al.* obtained a similar result in ref. [25], where, during magnetic sputtering of the film, a relationship between the gas pressure during deposition with the film conductivity and sensitivity to O$_2$ was found, along with the detector's response time. Baban *et al.* examined a sensor resistance change to different concentration of oxygen in gas mixture (Fig. 1) [26]. Li *et al.* in ref. [27] examined the ability to detect oxygen by Ga$_2$O$_3$ detectors with Ce, W and Zn impurities, the presence of which reduced the basic resistance and the operating temperature of the detector.
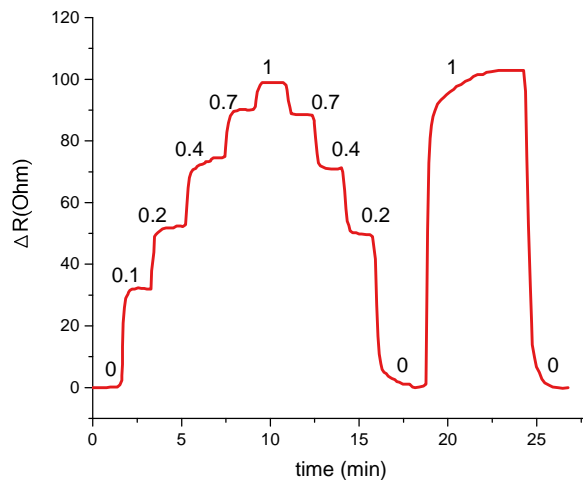


**Fig. 1.** Resistance change to different concentrations of oxygen in the O$_2$/N$_2$ mixture with a total flowing rate of 1 l/min, adapted from [26].
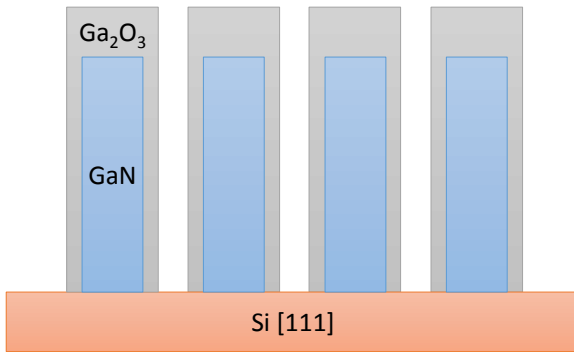
**Fig. 2.** The schematic of core/shell nanowires structure, adapted from [32].

Although the largest number of results has been shown for oxygen detectors, studies of the other gases sensors characteristics are known. Trinchi *et al.* in ref. [28] designed an H$_2$ sensitive Pt / Ga$_2$O$_3$ / SiC Schottky diode. The sensitivity of such a detector to small fractions of hydrogen (up to 0.06%) in synthetic air and pure N$_2$ atmospheres with 5% O$_2$ was shown. The detector relaxation time was also observed to decrease by a factor of 4 with an increase in temperature from 210 °C to 630 °C. The investigation results was reported of a hydrogen detector with high selectivity at an operating temperature of 700 °C [29]. This selectivity was achieved by sputtering a thin SiO$_2$ film on gallium oxide. In the presence of such a film, the sensitivity to gases with reducing properties is strongly suppressed, except for ethanol and acetone, for which the sensitivity is 10 and 4 times lower, respectively. It is shown that SnO$_2$ is a good material for doping gallium oxide films, which increases its conductivity by two orders of magnitude and, consequently, the sensitivity of the gas detector. Increased conductivity allows to reduce the size of the detector.

The modification of gallium oxide by inclusions of reduced graphene oxide discussed in ref. [30]. Such modification leads to a greater sensitivity to H$_2$S, relative to NH$_3$, SO$_2$, CO$_2$ and CO – at a concentration of 3 ppm, the sensitivity to H$_2$S is ~ 2 times higher compared to other reduced gases. The created detector is capable to operate at a temperature of 100 °C. It was also shown that the presence of H$_2$S gas strongly changes the ohmic resistance of the Ga$_2$O$_3$ grain boundaries. In order to increase devices environmental friendliness Pohle *et al.* in ref. [31] demonstrated a power consumption reduction from 900 mW, corresponding to ceramic analogs, to 20 mW for the developed gas detector microelectromechanical system (MEMS). The detector has also been modified by applying porous ceramics to the sensing element so increase in the CO and hydrocarbons sensitivity is achieved. Thus, resistivity ratio

$R_0/R_{gas}$ for ethanol concentration of 30 ppm was 20 and for 100 ppm was 45.

The increase in the CO and hydrocarbons sensitivity has been achieved due to sensing element modification by using porous ceramics.

In the future, it will be possible to utilize one-dimensional structures in gas detectors, such as nanorods or nanowires. So, Bui *et al.* in ref. [32] considered the synthesis of GaN / Ga$_2$O$_3$ core / shell nanowires with different thicknesses of the formed oxide film from 1 to 14 nm (Fig. 2). Wires utilization allows to increase the detector's CO sensitivity, response time and spatial resolution. The main advantage of one-dimensional structures is a larger surface area to volume ratio. Their size is commensurate with gas molecules, which makes it possible to create nano-detectors. Also, one-dimensional structures have the best mechanical properties: flexibility, reliability and resistance to mechanical stress. Liu *et al.* in ref. [33] designed a detector of O$_2$ and CO on Ga$_2$O$_3$ nanowires operating at temperatures of 100-500 °C. The peak sensitivity of oxygen is observed at a temperature of 300 °C, carbon monoxide - 200 °C. The detector selectivity was found only for CO sensitivity to which is 4 times larger than other gases with reducing properties. At the same time Jin *et al.* in ref. [34] investigated NO$_2$ detection by a Ga$_2$O$_3$-ZnO core / shell based sensor. The resulting nanorods showed a sensitivity 355 times higher than for Ga$_2$O$_3$ nanorods without a shell at a temperature of 300 °C and a concentration of 100 ppm. Mazeina *et al.* in ref. [35] reported the first capacitive gas detector based on Ga$_2$O$_3$ nanowire. Moreover, the surface of the nanowires was modified with pyruvic acid, the absorption of which reduces the detector's sensitivity to nitromethane and acetone (by 5 and 10 times, respectively), but increases the sensitivity to triethylamine by an order of magnitude. Capacity relation $C_0/C_{gas}$ of modified and initial nanowires were $3 \cdot 10^{-3}$ and $2 10^{-4}$ respectively. It is noteworthy that Ga$_2$O$_3$ wires can be returned to their original state before exposure to pyruvic acid by washing in water or heating.

Thus, Ga$_2$O$_3$ thin films and one-dimensional structures can be utilized to create sensors for both oxygen and other gases with high stability. High temperature stability was achieved in several gas detector implementations [28,29,33,34] making sensors based on Ga$_2$O$_3$ available for use in industrial furnaces or internal combustion engine. A detailed comparison of the gallium oxide gas sensors characteristics is presented in ref. [36].

## 4. LUMINESCENT DEVICES

In recent years, the possibility of gallium oxide utilizing in order to create displays and fluorescent lamps has

been actively examined. The various dopants utilization makes it possible to achieve emission in a different spectral range, and $Ga_2O_3$ high electric field strength allows to apply high electric fields to $Ga_2O_3$-based luminescent devices. To date, the results of the gallium oxide with various dopants luminescence spectra investigations and the results of the phosphorous characteristics studying have been obtained, however, the finished emitting devices have not yet been reported.

Frodason *et al.* in ref. [37] calculated the gallium oxide luminescence lines and optical transition energies for acceptor dopants: Mg, Be, Ca, Cd, Zn, Li, and N. Thus, the lines for Mg, Ca, Cd and Zn have a maximum in the range 2.15-2.62 eV (green / blue), when for Be and Li the peaks are in the region of lower energies - 1.71 and 1.56 eV (IR / red), respectively. It was also found that when the acceptor has a bond with one H, the luminescence band is not passivated, but the intensity peak is shifted.

Excited by X-rays luminescence of $β$-$Ga_2O_3$ and its temperature dependence was investigated by Tang *et al.* in ref. [38]. The recombination of free electrons and self-trapped holes (STHs) was found responsible for luminescence in the ultraviolet range. The results of the samples transmission spectrum measurements showed that the electron concentration decreases. This can be attributed to an increase in the number of gallium vacancies upon annealing in an atmosphere with a high oxygen concentration. The authors also question the n-type conductivity of gallium oxide: the version that oxygen vacancies are responsible for this type of conductivity is not confirmed, since the calculated ionization energy exceeding 1 eV cannot contribute to the n-type conductivity.

Yu *et al.* in ref. [39] studied the effect of Ta:$β$-$Ga_2O_3$ crystal transmission increment after annealing. The carriers concentration and the band gap after annealing in an air atmosphere decrease, while after annealing in a nitrogen atmosphere, on the contrary, they increase. Additionally, after annealing in air, the intensity of the blue and ultraviolet lines enhanced.

Huynh *et al.* in ref. [40] discussed in detail the effect of red luminescence in hydrogen doped gallium oxide. Inclusion of hydrogen in the $β$-$Ga_2O_3$ structure decreases layer resistance from $10^{10}$ $Ω$ / sq to $4·10^8$ $Ω$ / sq at 300 K. A high-valence gallium oxide with a binding energy 533.4 eV if hydrogen doping is present, H-radicals are absorbed in $β$-$Ga_2O_3$ and form strong bonds with oxygen atoms. Cathodoluminescence examination of the sample led to the red line at 1.9 eV.

Luchechko *et al.* in ref. [41] reported the results of temperature-stimulated luminescence and conductivity study of $β$-$Ga_2O_3$ crystals. During the work, three peaks were found at low temperatures: 116, 147, and 165 K.

The trap levels depths for these temperatures are, respectively, 0.15, 0.2, and 0.3 eV. These levels were attributed to the presence of interstitial gallium atoms. At high temperatures, 3 peaks were also found - 354, 385, and 430 K with the corresponding energies of 0.84, 1.0, 1.1 eV, which associated with the activation energy of oxygen vacancies.

Polyakov *et al.* in ref. [42] studied the electrical properties and luminescence in a bulk Fe:$β$-$Ga_2O_3$ crystal. During the work two lines of 1.78 and 1.8 eV were registered for the first time, and were attributed to the 'spin-flip' transition in $Fe^{3+}$. The band gap of about 850 nm (1.46 eV) is too large to an intracenter transition so its nature is not yet completely clear: either strong relaxation of the lattice or donor-acceptor recombination are probable.

Latter Polyakov *et al.* in ref. [43] also investigated analogous properties in the Mg:$β$-$Ga_2O_3$ Czochralski-grown crystal. The activation energy for the hole trap associated with Mg was determined - 1.05 eV. The multi-cathodoluminescence spectrum showed the presence of energies of 3.1, 2.81 and 2.56 eV.

The luminescence of glasses and glass ceramics MgO-$Ga_2O_3$-$SiO_2$ doped with $Mn^{2+}$ / $Eu^{2+}$ / $Er^{3+}$ was examined in ref. [44]. Peaks corresponding to the excitation of the dopant atoms were found during the luminescence study of the samples obtained by the sol-gel method. A two-photon process was also detected for samples with $Er^{3+}$. Energy transfer from europium ions to manganese is observed for the sample which contains these two ions. With an increase in the concentration of the $Eu^{2+}$, this effect is enhanced. Ueda *et al.* in ref. [45] examined orange luminescence and photodarkening, which depend on paramagnetic effects in undoped CaO $Ga_2O_3$-$GeO_2$ glass. The orange luminescence was associated with recombination between two defects in the glass: a nonbridging oxygen hole center and an unpaired electron at Ge ion bonding three oxygen. When a sample is irradiated with 290 nm at a temperature of 200 K, a shallow trap is efficiently generated. For 400 K, the wavelength for the shallow trap generation was 260 nm.

Jiang *et al.* in ref. [46] investigated one-dimensional structures of $Ga_2O_3$ doped with Li. The spectrum shift towards short wavelengths for obtained sample was found. Also, a highly intense red luminescence line centered at 692 nm is present for this sample (Fig. 3). Jiang *et al.* in ref. [47] synthesized and studied Zn-doped $Ga_2O_3$ nanostructures. The photoluminescence spectrum of the doped sample is shifted to longer wavelengths (Fig. 4). Doping with zinc to a certain level increases the luminescence intensity; however, when the threshold value is reached, the intensity declines strongly, which is associated with a decrease in the
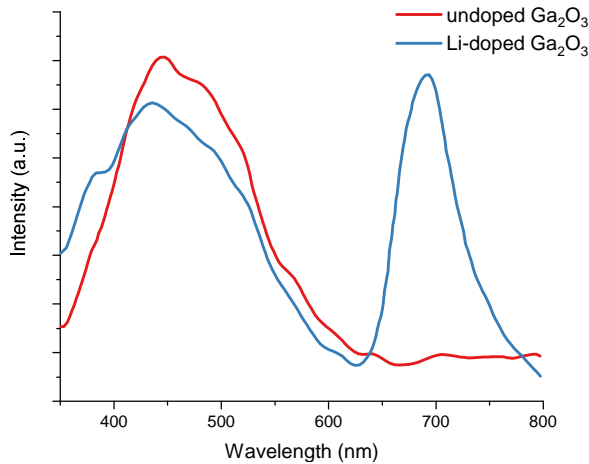
**Fig. 3.** The PL spectrum of the Li-doped and "undoped" Ga₂O₃ 1D nanostructures at room temperature, adapted from [46].
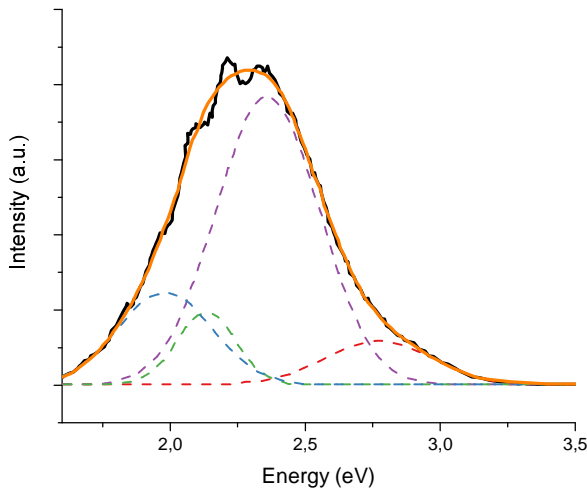


**Fig. 4.** Deconvoluted PL spectrum of the Zn-doped Ga₂O₃ nanostructure using Gaussian function, adapted from [47].

structure crystallinity and rise in the number of oxygen vacancies.

Thus, a large number of results reported for Ga₂O₃ multicolor emission in visible and IR range with different dopants. IR, red and yellow emission obtained for Be, Li, Cr, Co, Sm, Tm, Ce, Sn activated Ga₂O₃, green and blue – Mn, Tb, Er, Ho, Dy.

## 5. SCHOTTKY BARRIER DIODES

Schottky barrier diodes (SBD) attracted much attention as rectifying and switching devices due to fast reverse recovery and low forward voltage drop. Unique gallium oxide wide bandgap and high breakdown voltage provides SBD manufacturing to meet the modern high power electronics needs. Thus, the breakdown field of Ga₂O₃ 8 MV/cm exceeds these values of 4H-SiC and GaN – 2.5 and 3.3 MV/cm consequently. However, diamond surpasses Ga₂O₃ – 10 MV/cm, but today maximum
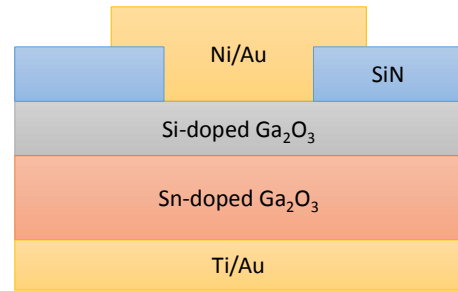


**Fig. 5.** Schematic vertical Ni/Au Schottky rectifier structure with edge-termination, adapted from [48].

diamond substrate size is about 20 mm when Ga₂O₃ 4-inch substrates are already available. Developing areas in SBD manufacturing are temperature stability increasing, modernizing devices characteristics on nanostructures and nanomembranes, investigating the Schottky barriers parameters with various contacts. Schematic vertical Ni/Au Schottky rectifier structure [48] is presented in Fig. 5.

Hou *et al.* in ref. [49] fabricated a IrO$_x$ / β-Ga₂O₃ Schottky contact, which demonstrates high temperature stability from 24 to 350 °C, while maintaining a low leakage current value - 5·10⁻⁹ at 350 °C and -3V and a high rectification factor of about 10¹⁰. Schottky barrier height and the ideality factor was 2.05 eV and 1.05, respectively. The thickness of the iridium oxide film obtained by magnetron sputtering was 35 nm. It was noted that during the first heating, the Schottky barrier height increases, and the ideality factor shows opposite dynamic. After cooling these characteristics remain at the same level as at 350 °C. This was explained by an increased work function during the oxidation of iridium oxide, and also, probably, an improvement in the ohmic contact of the diode. Swinnich *et al.* in ref. [50] reported flexible Schottky diodes on a plastic substrate (polymide) using β-Ga₂O₃ nanomembranes. The obtained nanomembranes have a similar band gap, but different energy of electron affinity and Raman characteristics in comparison with bulk β-Ga₂O₃ crystal. Diodes obtained by micro transfer printing technique demonstrate a record breakdown voltage of 1.2 MV/cm without elastic stress and 1.07 MV/cm in bending. A Schottky diode on a SiO₂ substrate has a breakdown voltage higher than polymide substrate diode: -136 V and -119 V, respectively. Electrical characteristics deterioration can be attributed to cracks in the crystal structure, which appeared as a result of bending. Original characteristics restoration is possible with low-temperature annealing. Sasaki *et al.* in ref. [51] pioneered the fluted metal-oxide-semiconductor (MOS) Schottky diode (Fig. 6). A Si-doped Ga₂O₃ layer on a Sn-doped β-Ga₂O₃ substrate was grown by chloride – hydride gas-phase epitaxy with an HfO₂ dielectric film. The breakdown voltage for the resulting
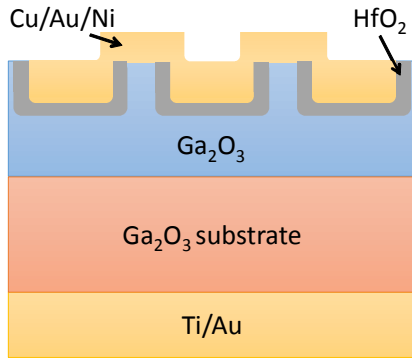
**Fig. 6.** First demonstration of trench MOS-type Schottky diode, adapted from [51].



**Fig. 7.** Current density-voltage characteristics of 200 μm diameter $Ga_2O_3$ based rectifiers fabricated with Ni/Au and W/Au as Schottky metal contact, adapted from [57].



**Fig. 8.** Cross-section of the vertical Schottky rectifier with W contacts, adapted from [58].

structure was 240 V. The ideality factor and the Schottky barrier height were 1.1 and 1.07 eV, respectively. The resulting device has a reverse-biased leakage current several orders of magnitude less than that of a conventional diode without trenches. Harada *et al.* in ref. [52] implemented a Schottky diode on the $PdCoO_2/\beta$-$Ga_2O_3$ contact, with a barrier height of 1.8 eV. The $I_{on}/I_{off}$ ratio is over $10^8$ even at 350 °C. A $PdCoO_2$ layer 20 nm thick was obtained by pulsed laser deposition. The created diode is ideal for use in harsh environments due to its stability at high temperatures (up to 800 °C), resistance to chemicals (acids/bases, pH from 0 to 14) and mechanical stress. Huang *et al.* in ref. [53] developed a Schottky diode with trenches with pre-optimized corner radii. The simulation results show that the breakdown voltage up to a certain moment increases with an increase in the trench corner radius and its length. Various dielectric materials influence was also investigated: $Al_2O_3$, $HfO_2$, and $SiO_2$. When using the first two, the breakdown voltage is 3.49 kV which surpasses most of the known results, when $SiO_2$ reduces this value by more than 2 times. Müller *et al.* in ref. [54] obtained high quality Schottky diodes on $SiO_2$ glass substrates. For growth temperatures below 510 °C, the obtained $\beta$-$Ga_2O_3$ films are amorphous and do not conduct electric current. For temperatures above 510 °C, the films become polycrystalline and conductive. The gallium oxide buffer layer obtained at 20! and annealed at 1100 °C showed the highest conductivity of 890 S/m. Additional heat treatment increases the grain size of the polycrystal, leading to higher conductivity, but also to a greater surface roughness. Thus, the control of the buffer layer electrical characteristics provides additional opportunities when manufacturing devices based on $\beta$-$Ga_2O_3$.

Farzana *et al.* in ref. [55] considered 4 metals as a Schottky contact with $\beta$-$Ga_2O_3$: Pd, Ni, Pt and Au. All Schottky contacts, 8 nm thick, were deposited by electron beam sputtering on commercial gallium oxide substrates. As a result of measuring the diodes *I-V* characteristics, the ideality factor was determined, which is in the range from 1.03 to 1.09. Schottky barrier heights were 1.27 V, 1.54 V, 1.58 V and 1.71 V for used metals, respectively. For Pd, Ni, Pt, excellent diode properties are observed, as described by the thermionic theory. Imperfect Schottky contact was obtained for gold due to uneven film thickness. Jiang *et al.* in ref. [56] also examined various metals for Schottky contact. The W, Mo, Au, and Ni were deposited onto an n-type $\beta$-$Ga_2O_3$ substrate grown by the Czochralski method. For the diodes under study, the *I–V* characteristics were measured, according to which the barrier height and ideality coefficient were determined, which amounted to 1.38 eV, 1.21 eV, 1.02 eV, 1.00 eV and 1.31, 1.05, 1.23, 1.05 for Au, Ni, W, Mo, respectively. Xian *et al.* in ref. [57] discussed in detail the effect of annealing W/$\beta$-$Ga_2O_3$ Schottky diodes (Fig. 7), which turned out to be stable at temperatures up to 500 °C. However, for high temperatures (550-600°), the leakage current increased by 2 orders of magnitude. The resulting Schottky W/Au contact showed excellent switching characteristics at a 300 V bias: the current flowing through the diode was 1.2 A, the recovery time – 100 ns. Received device $I_{on}/I_{off}$ greater than $10^6$ at -100 V bias current. The tungsten and nickel Schottky contacts with $\beta$-$Ga_2O_3$ were compared by Fares *et al.* in ref. [58]. Simple vertical geometry of Schottky
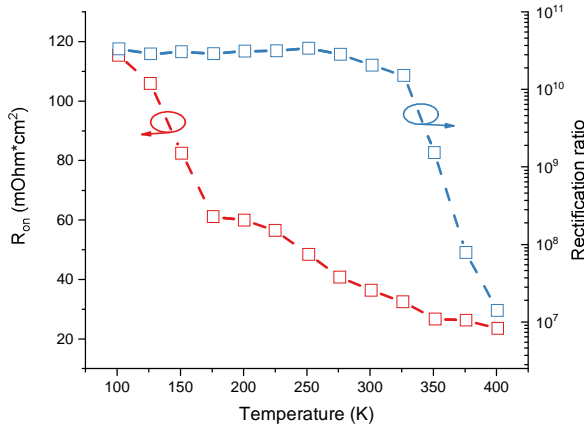
**Fig. 9.** Temperature dependence of $R_{on}$ and rectification ratio of the Au/Ni/β-Ga₂O₃ Schottky diode, adapted from [59].

diode is implemented in the research (Fig. 8). Ga atoms were found to migrate across the contact, slightly decreasing the Schottky barrier height after each heating. The Schottky barrier height for W was 0.97 eV and 0.39 eV at temperatures of 25 and 500 °C, respectively. Tungsten contact turned out to be more stable than nickel at a temperature 500 °C. In the article a comparative table for devices with Ni and W contacts is also provided.

Nickel is the most common contact used to create Schottky contact with gallium oxide, various growth techniques with different substrates and substrate crystallographic planes were discussed in detail. The influence of alfa-radiation and crystal structure defects were also investigated. Thus, Reddy *et al.* in ref. [59] implemented an Au/Ni/β-Ga₂O₃ Schottky diode (Fig. 9), which showed a strong temperature dependence of the Schottky barrier height and ideality coefficient. Experimental measurements have shown the existence of a double Gaussian distribution of the Schottky barrier heights with a transition at 225 K. The Schottky contact was deposited by electron beam evaporation (EBE) - 30 nm Ni and 250 nm Au. Ideality coefficient, barrier height and rectification coefficient when changing temperature from 100 K to 400 K varied from 2.76 to 1.05; from 0.4 to 1.13 eV; from $3.36 \cdot 10^{10}$ to $1.35 \cdot 10^7$. Jian *et al.* in ref. [60] showed trench Schottky diodes (Ni/β-Ga₂O₃) obtained by chloride-hydride gas phase epitaxy, which showed an $I_{on}/I_{off}$ ratio of $10^5$ at 650 K, and $10^{10}$ at room temperature. Also, when cooled to room temperature, the *I-V* characteristic is restored when a similar diode without trenches remains damaged. For a sample with trenches, the breakdown voltage was 1084 V. The high temperature stability of the obtained sample is attributed to the fact that when current flows through the trenches, the degradation of the structure decreases. Li *et al.* in ref. [61] implemented Ni/β-Ga₂O₃ Schottky diodes with reverse-biased leakage currents, with the effect of

tunneling through the Schottky barrier dominating over the entire breakdown voltages range from 0.8 MV/cm to 3.4 MV/cm. The experimental curves almost perfectly coincide with the calculated dependences according to the thermionic emission model, the value of the ideality coefficient was 1.022. It is also argued that Ga₂O₃ *p-n* homojunctions are not necessary, since high-quality *p-n* heterojunctions with a high built-in potential are excellent for manufacturing power elements. Kasu *et al.* in ref. [62] investigated the relationship between the defects of a Ni/Au/β-Ga₂O₃ (01$\overline{0}$) crystal and the Schottky barrier leakage current. Comparing the leakage current, dislocation density and void etch pit density, it was discovered that not all types of vacancies contribute to the leakage current. The diode leakage current is found to be related with the dislocations: dislocations parallel to [010] act as the directions of the leakage currents in the Schottky diode. Research results also indicate that unintentional Si doping has no effect on the leakage current.

The analogous reseach was held by Kasu *et al.* in ref. [63] who studied a Ni/Au Schottky diode based on (2$\overline{0}$1) β-Ga₂O₃. No clear relationship was found between the linear [010] defect, an arrow-shaped defect pointing in the [102] direction, a pumpkin-shaped defect also pointing in the [102] direction and the diode leakage current. The lack of a clear relationship was explained by the fact that threading dislocations are mainly located along [010] and do not pass through the (2$\overline{0}$1) plane. Despite the dislocation density of Schottky diodes on the (201) plane is higher than that of diodes on the (010) plane, the leakage current of diodes (2$\overline{0}$1) is still less. Oshima *et al.* in ref. [64] examined a Ni/Au Schottky diode on (001) β-Ga₂O₃: leakage current, ideality factor, and barrier height were considered. The detected linear defects do not change these characteristics, since they rarely go out to the (001) plane, being located along a direction parallel to it [010]. Vertical and horizontal Ni/Au Schottky diodes on β-Ga₂O₃ were studied by Khan *et al.* in ref. [65]. The horizontal structure can handle higher voltages than the vertical structure, but has a higher series resistance due to the diode geometry. The measured Schottky barrier height was 1.25 eV. The calculated breakdown field was $2 \cdot 10^5$ V/cm, which is an order of magnitude less than that of existing similar devices. This discrepancy in the values was explained by the low quality of the β-Ga₂O₃ film. Lingaparthi *et al.* in ref. [66] examined a Ni/Au vertical Schottky diode on β-Ga₂O₃, obtained by chloride-hydride gas-phase epitaxy, in which the leakage current at reverse bias was anomalously high. This effect was explained by introducing a thin surface barrier model, due to the high density of oxygen vacancies. Annealing in an N₂/O₂ atmosphere (80:20) lowered the leakage current

density by $10^2$ and increased the Schottky barrier height from 1.192 eV to 1.452 eV.

The mechanisms of the influence of injected electrons and temperature on the hole mobility in Ni/Au β-$Ga_2O_3$ Schottky diodes, which were exposed to alpha irradiation, were investigated by Modak *et al.* in ref. [67]. The electron activation energy for an irradiated sample was 49 meV, while for a sample not exposed to alpha particles it was 74 meV. Upon α-irradiation the recombination centers are formed near the conduction band which decreases activation energy of the sample. It was assumed that oxygen vacancies function as these centers. Konishi *et al.* in ref. [68] manufactured a Pt/Ti/Au vertical Schottky diode based on gallium oxide, the breakdown voltage of which exceeds 1 kV. The ideality factor of the device obtained by chloride-hydride gasphase epitaxy was 1.03 at 20-200 °C. The obtained Schottky barrier height exceeds the theoretical value, which is probably due to the presence of fluorine in $Ga_2O_3$. Lu *et al.* in ref. [69] investigated Pt/Ti/Au Schottky diodes with increased breakdown voltage and high switching speed. The device with an aperture obtained by ion implantation showed a decrease in the leakage current by $10^3$ and an increase in the breakdown voltage by a factor of 1.5. Reverse recovery time was 14.1 ns, which is better than a silicon pulse diode (FRD).

The effect of the nitrogen atoms concentration on the β-$Ga_2O_3$ thin films electrical and structural characteristics was studied by Luan *et al.* in ref. [70]. With an increase in the nitrogen concentration, the crystal structure degrades, and the formation of a polycrystalline structure is possible. After annealing in an argon atmosphere, the crystal quality is partially restored. The carrier concentration was measured for Ti/Au Schottky diodes which were obtained on the basis of $Ga_2O_3$: N/n-$Ga_2O_3$. Upon nitrogen implantation, the carrier concentration smoothly decreases by 1–2 orders of magnitude. Lu *et al.* in ref. [71] reported the possibility of X-ray detection by a vertical Pt/Au Schottky diode based on a bulk β-$Ga_2O_3$. The obtained detector photosensitivity was 1.8 µC/Gy at a bias voltage of -25.8 V, the response time – 10 s. It was found that the presence of oxygen vacancies in the β-$Ga_2O_3$ crystal degrades the detector sensitivity and response rate. Zhou *et al.* in ref. [72] reported about the leakage current in the Pt/β-$Ga_2O_3$ Schottky contact at temperatures from 300 to 425 K. The main mechanism of the leakage current was determined by the emission of electrons through charge traps located at the metal-semiconductor interface, which is described by the Poole – Frenkel theory. The energy of these charge traps is defined as 0.7 eV below the conduction band. Raad *et al.* in ref. [73] showed a high temperature inertia in a Schottky diode. Such results were achieved by thermoreflectance-based tomography

of the temperature distribution in vertical Schottky diode on β-$Ga_2O_3$. Pulse activated temperature distribution lags behind the shape of the activation pulse which is associated with the low gallium oxide thermal conductivity. Oda *et al.* in ref. [74] examined Schottky diodes Pt/α-$Ga_2O_3$. Gallium oxide layers were grown on sapphire substrates by gas-phase deposition, after which they were lifted off from the substrate. The resulting Schottky diodes showed series resistance and breakdown voltage of 0.1 mΩ·$cm^2$ and 531 V for the first sample and 0.4 mΩ·$cm^2$ and 855 V for the second one, respectively.

Yang *et al.* in ref. [75] created Schottky diodes on a bulk gallium oxide crystal doped with Sn. The rectifying contact material was Ni/Au, the contact diameter varied from 20 µm to 0.53 mm. For these diameters, breakdown voltages and series resistance of 1600 V and 25 mΩ·$cm^2$, 250 V and 1.6 mΩ·$cm^2$ were obtained. $I_{on}/I_{off}$ ratio for the resulting diodes ranged from $3 \cdot 10^7$ to $2.5 \cdot 10^6$ at a bias of 1.3 V.

Schottky diodes based on $Ga_2O_3$ have already been described in detail. To achieve Schottky barrier oxides ($SiO_2$, $HfO_2$, IrO, $Al_2O_3$ and $PdCoO_2$) or metals (Pd, Ni, Pt, Au, W, Mo and Ti) are used. Current state of $Ga_2O_3$ Schottky diodes technology allows to fabricate samples with ideality coefficient value near 1. Structure modifications of such diodes are also objects of interest: ion implanted aperture or trench structure increase breakdown voltage of element. At room temperature created devices show rectification ratio up to $10^{10}$ and breakdown voltage over 1 kV. Comparative tables of metal/β-$Ga_2O_3$ and metal oxide/β-$Ga_2O_3$ compounds were given in supplementary materials of ref. [52]. The record achieved ideality factors are listed further: Au/Ni with *n* equal 1.00 and barrier height 1.2 eV, Pt with 1.03 and 1.53 eV, Pd with 1.05 and 1.29, Ni with 1.02 and 1.21 eV, Au/W with 1.04 and 0.97 eV. As for metal oxides, $AuO_x$ turns out to be the contact with the least ideality factor – 1.02 and barrier of 1.69 eV. Next oxides are $RuO_x$ with 1.05 and 1.59 eV, $PtO_x$ and $IrO_x$ with factor of 1.08 along with 1.06 eV and 1.78 eV consequently.

## 6. SOLAR-BLIND PHOTODETECTORS

$Ga_2O_3$ has attracted much attention recently, and its characteristics of solar-blind UV detection have been demonstrated in various device structures, including metal-semiconductor-metal (MSM) structure, Schottky junction, and heterojunction structure. MSM photodetectors are renowned for its fast response speed due low capacitance per unit area and low built-in electric field in the Schottky junction, as well as design simplicity and easy preparation. To effectively utilize solar-blind photodetectors in secure communication and space
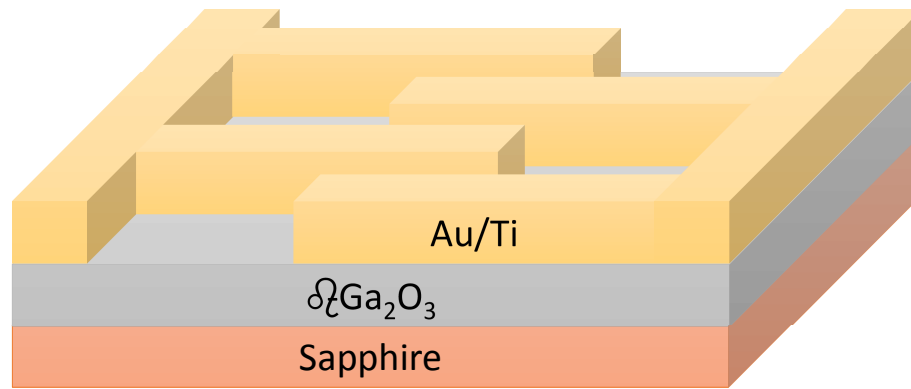
**Fig. 10.** Thin film MSM structure photodetector, adapted from [79].

detection fast response times and self-powered ability are strongly required. The vertical Schottky photodiode should satisfy this requirement. Although great progress has been made in Ga$_2$O$_3$ photodetectors, the responsivity remains relatively low [76]. On the other hand, Schottky photodiodes have many advantages over MSM photodetectors, such as higher response speed and possible zero bias operation due to the built-in electric field, high quantum efficiency, low dark current, and high UV/dark current ratio because of the existence of Schottky barrier [77].

The first solar-blind photodetector based on Ga$_2$O$_3$ epitaxial layers obtained by metal organic chemical vapor deposition (MOCVD) was reported by Pavesi *et al.* in ref. [78]. The rise and decay times were 2 s. The implemented detector demonstrated a 3 orders of magnitude difference between illumination above / below the band gap. Using MBE Guo *et al.* in ref. [79] grew β-Ga$_2$O$_3$ on sapphire substrates at various oxygen pressures and ambient temperatures. Structure of implemented solar-blind detector is shown in Fig. 10. The best sample was obtained at $5 \cdot 10^{-3}$ Pa and 750°C. Based on this sample, a MSM photodetector was obtained that showed strong absorption at wavelengths less than 250 nm. The rise and decay times of the pulse were 0.86 and 16.61 s, respectively. Zhang *et al.* in ref. [80] fabricated an amorphous gallium oxide solar-blind MSM photodetector whose characteristics were tuned by the oxygen vacancy concentration. The resulting dark current, response time, photosensitivity and high UV-C/UV-A suppression ratios were 1 pA, 243.9 s, 55.5 A/W, and 10$^3$, respectively. Varying the oxygen flow during the film deposition makes it possible to change the amorphous gallium oxide conductivity, which subsequently leads to a change in the type of contact.

Chen *et al.* in ref. [81] showed a Schottky photodetector implemented on an Au/β-Ga$_2$O$_3$ nanowires array. At -30 V bias the device displays a low dark current of 10 pA. The estimated ideality factor and series resistance were 30 and 10$^8$ Ohm, which is explained by damage to the structure or by the non-conductive layer at the interface between the gold contact and gallium oxide. At 0 V bias the photodiode has a sensitivity of about 0.01 mA/W and a rejection ratio of 258 nm/280 nm is 11, while at 258 nm/400 nm it is 38. Photosensitivity in the non-solar-blind range and the poor quality of epitaxial structures due to the mismatch of the lattice parameter are problems that are inherent in existing photodetectors based on heterojunctions with gallium oxide. Guo in ref. [82] proposed to solve these problems when manufacturing a photodetector based on the phase transition of α- and β-Ga$_2$O$_3$. Investigation of the resulting nanorods array with a phase transition showed that photogenerated carriers can be effectively separated. Suzuki *et al.* in ref. [83] increased the Schottky photodiode sensitivity by 10$^2$ for wavelengths that are less than 260 nm by annealing at 400 K. The maximum photosensitivity was 10$^3$ A/W. The suppression coefficient of 240 nm/350 nm is equal to 10$^6$. The ideality coefficient after annealing approached one. Nakagomi *et al.* in ref. [84] demonstrated a Schottky photodiode based on a Ga$_2$O$_3$/SiC heterojunction by vaporizing gallium in an oxygen plasma. The rise and decay times of the pulse are 1.2 µs and 1.5 µs, respectively. The suppression ratio of 240 nm/350 nm is 130. Kong *et al.* in ref. [85] showed a Schottky photodiode based on graphene/gallium oxide heterostructure. The rise and decay times were 94.83 s and 219.19 s. The photosensitivity was 39.3 A/W, and the external quantum efficiency was $1.96 \cdot 10^4$. Photodetector based on another heterostructure – α-Ga$_2$O$_3$/ZnO was fabricated by Chen *et al.* in ref. [86]. An intermediate layer formation at the heterojunction was noted - diffused Ga and Zn atoms lead to bending of the energy bands boundaries, which affects the Schottky diode rectifying properties. The *I-V* characteristic was also simulated, which repeat the curves obtained by measuring. Also a solar-blind photodetector based on graphene/β-Ga$_2$O$_3$ heterostructure was demonstrated by Chen *et al.* in ref. [87]. The resulting radiation detector at zero bias voltage has a photosensitivity

of 10.3 mA/W (wavelength 254 nm), a UV/visible rejection ratio of $2.28 \cdot 10^2$ with rise and decay times of 30 ns and 2.24 µs, respectively. Such a low response time was explained by the high velocity of charge carriers in graphene and gallium oxide and a low number of defects at the graphene/β-$Ga_2O_3$ interface. The effect of the oxygen vacancies concentration on the β-$Ga_2O_3$/SiC heterostructure detector photosensitivity was discussed in detail by An *et al.* in ref. [88]. Presence of oxygen vacancies impairs the rectifying properties as well as the photosensitivity of the device. For the sample with the lowest oxygen vacancy content, a sensitivity of 6308% [$(I_{light} - I_{dark}) / I_{dark}$] (wavelength 254 nm) and a rectification factor of 1900 [forward/reverse currents] were obtained. Alema *et al.* in ref. [89] designed a solar-blind photodetector based on β-$Ga_2O_3$ with MOS-hydride epitaxy, which demonstrates a rectification factor of $10^8$ at 2 V bias. The diode ideality factor and breakdown voltage are 1.23 and 110 V. Suppression factor $10^4$. Photosensitivity 0.16 A/W at 222 nm with a bias voltage of 0 V, giving an external quantum efficiency of 87.5 %. Oshima *et al.* in ref. [90] showed a vertical photodetector grown on a gallium oxide substrate with rectification coefficients greater than $10^6$ at a bias voltage of 3 V. At a wavelength of 254 nm, its photosensitivity was 3.1 A/W. Cui *et al.* in ref. [91] explored a solar-blind photodetector based on amorphous gallium oxide grown on quartz and polyethylene naphthalate substrates. The detectors were obtained at various oxygen pressures, and the optimal value was determined at which a decrease in the oxygen vacancies number and an increase in the Schottky barrier height were observed. The detectors showed a pulse decay time of 19.1 µs and a photosensitivity of 0.19 A/W. At the same time, devices on a flexible substrate do not show degradation under elastic stresses.

Large values of photosensitivity and EQE can be achieved by creating solar-blind detectors on 2D nanostructures. Thus, Tian *et al.* in ref. [92] showed a solar-blind detector based on $Ga_2O_3$ nanobands doped with indium. The resulting photodetector demonstrated a high photosensitivity of $5.47 \cdot 10^2$ A/W, a quantum efficiency of $2.72 \cdot 10^5$ %, and a shorter rise/decay time of 1/0.6 s compared with a similar non-doped device based on $Ga_2O_3$ nanobands, and also with other doped photodetectors. Oh *et al.* in ref. [93] implemented a photodetector on a gallium oxide film obtained by mechanical exfoliation. The Schottky diode implemented on β-$Ga_2O_3$ showed a low dark current - $2.8 \cdot 10^{-13}$ and high sensitivity in the UV C range - 1.68 A/W. The suppression coefficient of 254 nm/365 nm was $1.92 \cdot 10^3$. The time response was 1.76 s for on and 0.53 s for off. Another solar-blind photodetector was obtained using the same technology Kim *et al.* in ref. [94], which demon-

strates a sensitivity of $1.8 \cdot 10^5$ and an external quantum efficiency of $8.8 \cdot 10^5$ at a bias voltage of -30 V. Zhong *et al.* in ref. [95] showed the implementation of a solar-blind photodetector with an average $Ga_2O_3$ plate thickness of 63 nm. The resulting device demonstrates high photosensitivity - 19.31 A/W and external quantum efficiency - 9427%, which surpass similar characteristics of detectors implemented on other nanostructures (nanowires and nanoribbons). Rise and decay times are about 20 ms. By magnetron sputtering a thin-film photodetector based on magnesium-doped $Ga_2O_3$ was obtained by Qian *et al* in ref. [96]. The obtained sample sensitivity is $8.7 \cdot 10^5$ %, the photosensitivity is 23.8 mA/W, the pulse decay time was 0.02 s. The authors reported that the dark current of the device (4.1 pA) is three orders of magnitude lower than that of the same samples of gallium oxide without doping. Also, a 1D nano-structures was utilized to avalanche photodetector fabrication by Zhao *et al.* in ref. [97] who reported about an ZnO/$Ga_2O_3$ core/shell microwires device. The photosensitivity at -10 V bias was $5.18 \cdot 10^3$ A/W, and the rise and decay times were 20 µs and 42 µs, respectively. Another avalanche PD was received using MOCVD by Ahn *et al.* in ref. [98]  The thermal dependences of its characteristics was examined: when changing from 25 to 350 °C, the photocurrent (wavelength 254 nm) varied from $2.5 \cdot 10^{-7}$ A to $2.2 \cdot 10^{-6}$ A, photosensitivity - from 5 to 36 A/W and external quantum efficiency from $2.5 \cdot 10^3$ to $1.75 \cdot 10^4$ %. Such high values are explained by the effect of charge carriers multiplication. Tak *et al.* in ref. [99] investigated the effect of gamma radiation on β-$Ga_2O_3$ solar-blind photodetector obtained with PLD. The dark current decreased from $3.27 \cdot 10^{-7}$ A to $1.88 \cdot 10^{-7}$ A. On the contrary, the Schottky barrier height was increased after irradiation, which is explained by an image-force lowering.

Gallium oxide solar-blind photodetectors spectral responsivity (Fig. 11) is presented in the review prepared by Xu *et al.* [100] along with solar-blind photodetectors technology current state general description.

## 7. MEMORY DEVICES

In the next generation nonvolatile memory, great attention is being paid to the resistive random access memory (RRAM) technology development gradually replacing the more traditional dynamic random access memory and flash memory. Resistance switching effect observed in RRAM consists in the appearance of conductive structures in the material, that can also be observed in gallium oxide. So, Lee *et al.* in ref. [101] implemented resistance switching of a $Ga_2O_3$ film doped with chromium, which create oxygen vacancies during diffusion
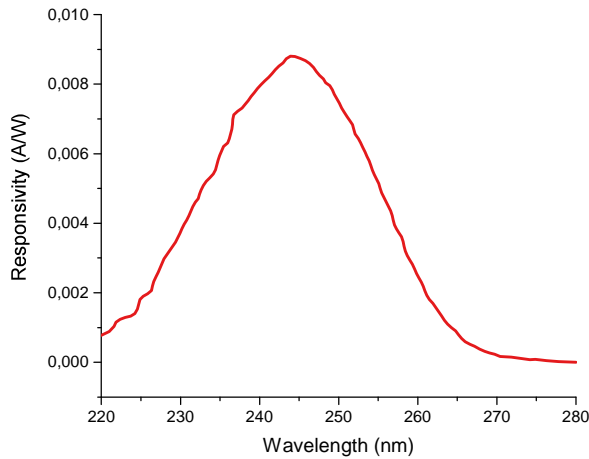
**Fig. 11.** Responsivity of Ga$_2$O$_3$ photodetector, adapted from [100].

into the structure. Varying the film size and the annealing temperature changes the structure resistance The films conductivity changing mechanism was associated with the formation/destruction of conducting objects at the interface between Ti and the Cr: Ga$_2$O$_3$ film. Hou *et al.* in ref. [102] investigated oxygen vacancies conducting filaments in β-Ga$_2$O$_3$. Three types of oxygen leaks have been found, which form filaments with different resistance values, which suggests the use of gallium oxide in multilevel memory cells. It was found that the conductive filaments are formed preferably in the direction [010].

Pan *et al.* in ref. [103] investigated ITO/Ga$_2$O$_3$: ITO/TiN structure resistance switching. The conduction mechanism can be realized both at the contact surface and during the formation of conducting fibers inside the structure. The obtained states with low and high conductivity are stable for 10$^4$ s at 85 °C, which, when extrapolated, gives 10 years of operation at room temperature. The presence of an additional Pt contact suppressed oxygen ions release which changed the resistance switching mechanism in the device. Yan *et al.* in ref. [104] showed bipolar resistance switching in the In-Ga-Zn-O/Ga$_2$O$_3$/In-Ga-Zn-O structure. The resulting device has a transmission of 91.7% in the visible range. With 200 switching cycles, the resistance value is still distinguishable for high and low conductivity modes - 280 and 20 kΩ, respectively. Zhi *et al.* in ref. [105] showed bipolar and unipolar changes in resistance in the Cu$_2$O/Ga$_2$O$_3$ structure and a controlled mechanism of transition between them (Fig. 12, Fig. 13). The voltages SET and RESET are around 4 and -6 V for bipolar switching. High resistance values are 10$^4$ Ω, while low values fluctuate between 46 and 210 Ω. Both resistances are stable for more than 10$^4$ s. Yang *et al.* in ref. [106] examined the oxygen concentration influence on the operation of resistive memory devices with random access Al/Ga$_2$O$_3$/
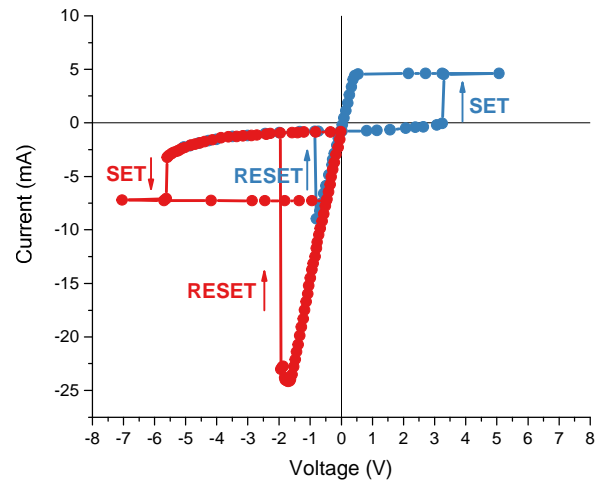


**Fig. 12.** Typical current-voltage curves for the bipolar resistive switching (blue curve) and unipolar switching (red curve), adapted from [105].
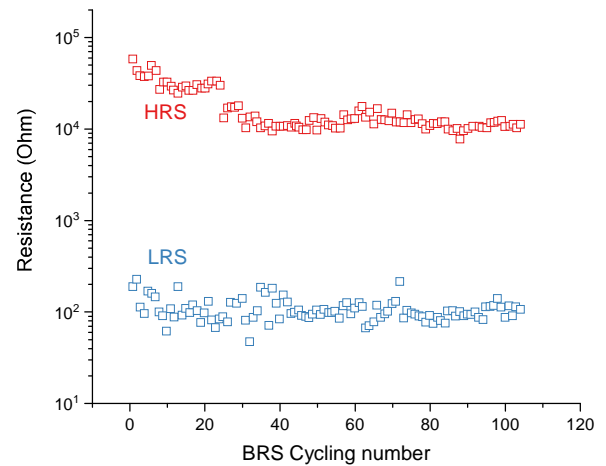


**Fig. 13.** Endurance property of the device in bipolar resistive switching mode, adapted from [105].
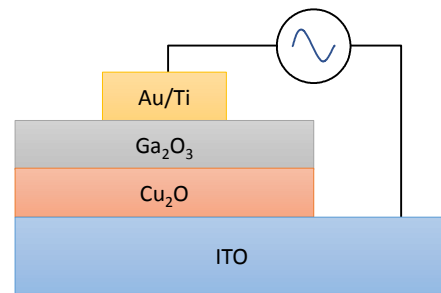


**Fig. 14.** RRAM device schematic structure, adapted from [109].

ITO. As a result, the sample with 25% oxygen showed the best result with the number of switching cycles equal to 220. The $I_{on}/I_{off}$ ratio was 5·10$^4$, the stability time was 10$^4$, and the high/low resistance ratio of the device was about 7·10$^5$. The SET and RESET voltages for the device were -1.68 and 0.45 V. Gan *et al.* in ref. [107] investigated the effect of temperature and annealing atmosphere on the switching properties of the Cu/TiW/Ga$_2$O$_3$/Pt memory device resistance. Annealing in nitrogen and

oxygen atmospheres decreases the values of the SET and RESET voltages. After annealing in a pure nitrogen ($N_2$) atmosphere, the devices showed an increase in memory area and an increase in stability when switching states. Zheng *et al.* in ref. [108] implemented a resistance switching memory device on the GZO-$Ga_2O_3$-ZnO-$Ga_2O_3$-GZO structure obtained by chemical vapor deposition of organometallic compounds. The manufactured device is 92% transparent in the visible range. The SET and RESET voltages for the device were -12 and 14 V. The high/low resistance ratio of the device was $10^2$ and both states are stable for $10^5$ s. Gan *et al.* in ref. [109] showed a resistance switching device (Fig. 14) with a Cu/TiW/IGZO/$Ga_2O_3$/Pt structure. The high/low resistance ratio exceeds $10^3$, the stability of states is observed for $10^4$ s at 85 °C. The SET and RESET voltages for such a device were 2.5 and -2 V, respectively. Gan *et al.* in ref. [107] examined the influence of annealing parameters on a memory device based on an amorphous gallium oxide layer. Annealing in a nitrogen atmosphere improves the device parameters. The high/low resistance ratio was $10^5$, with the number of switchings 750 at a temperature of 85 °C. The voltages SET and RESET ranged from 2.2 to 4 V and from -0.5 to -2 V, respectively. Shen *et al.* in ref. [110] showed bipolar resistance switching in the Pt/$Ga_2O_{3x}$/SiC/Pt structure. The voltages SET and RESET were 0.82-1.92 V and from -1.3 to -0.408 V, respectively, which is a 1.2 V the memory area, which is determined by the difference between the SET and RESET voltages, where there is no overlap between these states. The ratio of resistances in two states exceeds $10^3$, and their stability is observed for a time exceeding $10^4$ s. The article also provides a quick table comparing the different types of resistance switching devices.

There are also implementations of RRAM based on nanostructures. Thus, Weng *et al.* in ref. [111] showed resistance switching in β-$Ga_2O_3$ nanowires grown on a Si substrate. The average diameter of the resulting structure was 127 nm. The measurements were carried out for pure nanowires and for partially gold-plated ones. For the first, the SET and RESET voltages were 3.1 and -3.25 V, when, with partial gold plating, these values decrease to 1.87 and -1.9 V. Hsu *et al.* in ref. [112] showed bipolar resistance switching on a single Au-$Ga_2O_3$ nanowire (core/shell). The ratio of high and low resistance is greater than $10^3$, the SET-RESET voltages are 6 and -8.5 V. Tsai *et al.* in ref. [113] demonstrated the rapid synthesis of a memory device using local anodic oxidation under atomic force microscopy. For the obtained gallium oxide nanodots with a typical size of 300 nm, states with high and low resistance values were obtained, which amounted to 9.19 MΩ and 2.97 kΩ, respectively, which gives a difference of three orders of magnitude.

The capacitance memory device can also be based on the charge trap effect. So, Weng *et al.* in ref. [114] implemented a charge trap memory device based on $Ga_2O_3$ layers. The Au/$Ga_2O_3$/$SiO_2$/Si structure was obtained by magnetron sputtering and high-temperature annealing. Moreover, at different annealing temperatures, was different. So, the memory area was 1.6, 3, 4.8 and 1.5 V for annealing temperatures of 600, 680, 760 and 780 °C, respectively. The degradation of high and low capacitance states was 1% and 1.7% after $10^4$ s.

Thus, multilevel memory cells on $Ga_2O_3$ based heterostructures, nanodots and nanowires were shown recently with high/low resistance ratio ~ $10^3$, SET & RESET voltages not exeeding ±5V and stability over $10^4$ s. Most of the structures described were created by rf-magnetron sputtering. Promising area in RRAM manufacturing is transparent device construction with transmittance factor exceeding 90%.

## 8. FIELD EFFECT TRANSISTORS

There are results mentioned of various field-effect transistors producing: MOSFETs, MISFETs, MESFETs on different gallium oxide polymorphs and heterostructures. To meet the demands of the modern power electronics application areas, the high breakdown voltage with $I_{on}/I_{off}$ ratio and low leakage current is of great interest. The largest number of reports is aimed at improving these characteristics, increasing the FETs technological performance, modernizing the technology for growing gallium oxide layers and devices manufacturing. For example, Madadi *et al.* in ref. [115] carried out modeling of transistors in order to optimize the carriers distribution in the structure and increase a breakdown voltage, structure self-heating, parasitic capacitance and charge carriers concentration.

Implementing a tunnel diode to change the carrier distribution reduced the leakage current in the transistor saturation region. Tetzner *et al.* in ref. [116] studied the possibility of creating transistors with a large electric breakdown field. The devices demonstrated a threshold voltage, $I_{on}/I_{off}$ and a subthreshold slope of -3.6 V, $10^9$ and 200 mV/dec, respectively. The breakdown voltage reached a record value among similar devices and was about 1200 V. The main factor that lowers the breakdown voltage was the increased Si concentration between the β-$Ga_2O_3$ epitaxial layer and the substrate. Green *et al.* in ref. [117] implemented a MOSFET with a record transconductance of 21 mS/mm (Fig. 15, Fig. 16). Extrinsic cutoff frequency and maximum oscillating frequency were 3.3 and 12.9 GHz, respectively; $I_{on}/I_{off}$ was $10^6$. Operation in the radio frequency range is achieved by reducing the contact resistance by heavy doping in the contact area.
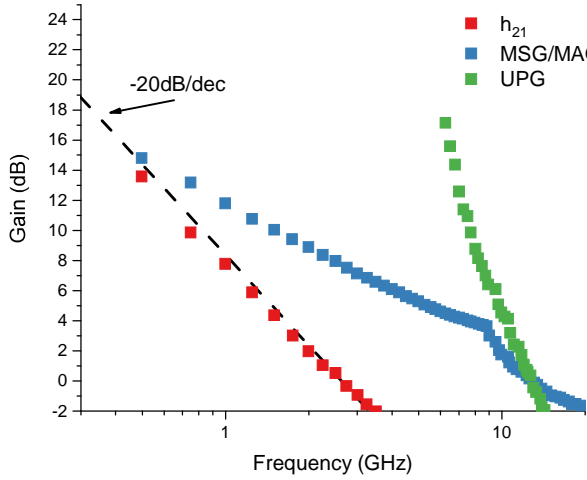
**Fig. 15.** Extrinsic small signal RF gain performance recorded at $V_{GS} = -3.5$ V (peak $g_m$) and $V_{DS} = 40$ V, adapted from [117].
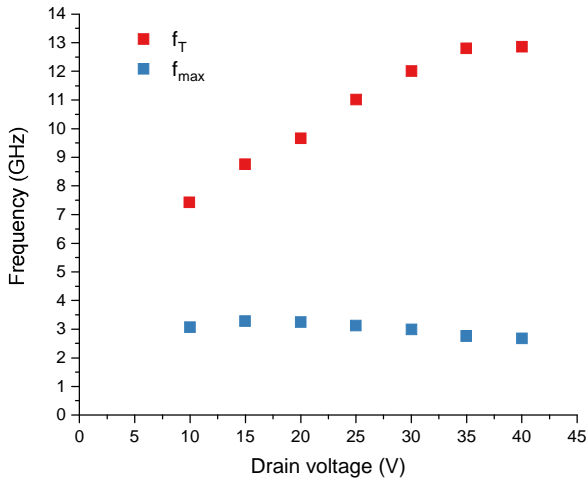


**Fig. 16.** Cutoff frequency ($f_T$) and maximum oscillating frequency ($f_{max}$) as a function of drain bias. Each measurement was taken with the gate contact biased with the gate voltage corresponding to peak transconductance, adapted from [117].

At the research initial stage, one often resorts to computer simulation of device performance, the results of which are widely reported. So, Kotecha *et al.* in ref. [118] simulated and analyzed a vertical MOSFET on β-Ga₂O₃. The study showed an inverse relationship between the threshold voltage and the current amplification, and their dependence on the device geometry and the acceptor concentration in the crystal. Also, the temperature dependences are investigated, and the released power during a short circuit failure of the transistor is studied. Lv *et al.* in ref. [119] performed a simulation and implemented a two field electrodes transistor with a breakdown voltage above 3000 V after the device annealing in an oxygen atmosphere. The developed MOSFET was grown using organometallic gas-phase epitaxy. The device threshold voltage was 4.1 V, $I_{on}/I_{off}$

about 10⁸. Park *et al.* in ref. [120] conducted a vertical transistor on Ga₂O₃ simulation. In particular, the source geometry was analyzed in detail and its significant influence on the device characteristics was found. The maximum drain current was 750 A/cm² with a gate bias of 3 V. For an optimized structure, $I_{on}/I_{off}$ exceeds 10⁸, the breakdown voltage is about 400 V.

For gallium oxide based heterostructures various results presented. Kim *et al.* in ref. [121] reported a field-effect transistor with a transition gate on the WSe₂-Ga₂O₃ heterostructure. A WSe₂ thin layer was deposited on a mechanically separated β-Ga₂O₃ plate, resulting in a high quality heterointerface. The $I_{on}/I_{off}$ ratio was 10⁸, the subthreshold slope - 133 mV/dec, the three-contact breakdown voltage - 144 V. Dang *et al.* in ref. [122] obtained a MESFET on *n* type α-Ga₂O₃ Schottky diode and AgO$_x$ by chemical vapor deposition. The rectification factor of a typical device and the breakdown voltage - 6·10⁶ and 19.6 V. Also, the transistors capable of withstanding voltages up to 48 V were implemented. The $I_{on}/I_{off}$ ratio was 2·10⁷. The resulting device is transparent in the visible range. Kim *et al.* in ref. [123] studied MISFET on the h BN/β-Ga₂O₃ heterostructure. h-BN has a clean and smooth surface and does not introduce discontinuities in the charge density at the interface with gallium oxide, which allows to obtain better transistor characteristics such as $I_{on}/I_{off}$ ratio, subthreshold slope and threshold voltage. These values for the device were respectively 10⁶, 502 mV/dec and -48 V. Tadjer *et al.* in ref. [10] showed the first MOSFET with β-Ga₂O₃ epitaxial layers obtained at high growth rates during MOCVD. For the devices obtained, a record carrier mobility was 170 cm/(V·s), which is superior to the results previously shown for Ga₂O₃-based devices. $I_{on}/I_{off}$ value was 10⁸, threshold voltage -15 V. Yadava *et al.* in ref. [124] was the first to propose a transistor device on a β-Ga₂O₃/black phosphorus heterostructure. MOSFET was tested for operation at high frequencies. The maximum drain current was 43.15 mA/mm, the power gain was 15.3 dB, the output power was 15.11 dBm, and the efficiency was 3%. The $I_{on}/I_{off}$ ratio is greater than 10¹⁰. Higashiwaki *et al.* in ref. [11] showed a transistor grown on a Ga₂O₃ (010) substrate by molecular beam epitaxy. The device three-contact breakdown voltage was greater than 250 V when the leakage current was 3 µA. The $I_{on}/I_{off}$ ratio is approximately 10⁴. Xia *et al.* in ref. [125] obtained a MESFET on β-Ga₂O₃ with ohmic contacts on an additionally grown β-Ga₂O₃ layer, leading to reduce the longitudinal contact resistance to 1.5 Ω/mm. The resulting transistor has a peak drain current of 140 mA/mm, a three-contact breakdown voltage of 170 V. $I_{on}/I_{off}$ was 10⁵. Kim *et al.* in ref. [126] investigated the properties of MESFET on annealed β-Ga₂O₃ with Pt/Au Schottky contacts. The resulting transistor on a micro-

layer of gallium oxide showed performance up to 700 °C, after which the Schottky contact breakdown begins. Above 800 °C, the Pt/Au contact exhibits the ohmic contact properties. Authors also obtained the dependencies of the $I_{on}/I_{off}$ ratio, the Schottky barrier height, and the transmissibility from the annealing temperature. Matsuzaki *et al.* in ref. [127] examined a MISFET on a gallium oxide epitaxial layer. The grown films with a band gap of 4.9 eV are transparent from the near-IR to far-UV ranges. Crystalline structure of epitaxial film was different from β-$Ga_2O_3$ and showed high conductivity. The resulting transistor has a threshold voltage of -6.7 V and a drift mobility of $5 \cdot 10^{-2}$ cm²/(V·s). Zhang *et al.* in ref. [128] demonstrated a field-effect transistor on a double heterostructure β-$(Al_xGa_{1-x})_2O_3/Ga_2O_3$ with a quantum well. The device has a maximum leakage current of 257 mA/mm, a transconductance of 39 mS/mm, and a breakdown voltage of 428 V. Ahmadi *et al.* in ref. [129] showed a transistor on the β-$(Al_xGa_{1-x})_2O_3/$β-$Ga_2O_3/(Al_xGa_{1-x})_2O_3$ heterostructure obtained by molecular beam epitaxy. Authors also investigated the effect of Ga polishing on the surface morphology and the concentration of unintentionally doped Si atoms. The maximum current density was 20 mA/mm and the transconductance was 4 mS/mm. $I_{on}/I_{off}$ ratio exceeded $10^9$ for polished and unpolished samples. Higashiwaki *et al.* in ref. [130] grew a MOSFET by molecular beam epitaxy on a â-$Ga_2O_3$ (010) substrate and examined the resulting device performance at different temperatures. To obtain ohmic contacts, gallium oxide was doped with Si. The $I_{on}/I_{off}$ ratio for the transistor is greater than $10^{10}$; the three-pin breakdown voltage was 370 V; the maximum drain current at 4 V bias was 39 mA/mm. The resulting devices can operate up to 250 °C without permanent changes in structure and characteristics. Moser *et al.* in ref. [131] designed a β-$Ga_2O_3$ based transistor with a record current density exceeding 450 mA/mm. The carrier concentration influence on the resulting MOSFET electrical parameters was investigated. An analytical model with voltage correction factor that accurately predicted the performance for all doping variations was built. The $I_{on}/I_{off}$ ratio was $10^{8.6}$. Later, Moser *et al.* in ref. [132] showed a Ge-doped β-$Ga_2O_3$ transistor grown by molecular beam epitaxy. The $I_{on}/I_{off}$ ratio was $10^8$, the drain current exceeded 75 mA/mm at zero bias ($V_g = 0$), and the breakdown voltage was 479 V. The measured carrier mobility was 111 cm²/(V·s). Also, the work presents a short table comparing the parameters of existing MOSFET. Recently, Moser *et al.* in ref. [133] received a MOSFET with an L-shaped contact with a maximum transducer gain, maximum output power, and peak power added efficiency of 13 dB (15 dB), 715 mW/mm (487 mW/mm), and 23.4% (21.2%), respectively, at frequencies of 1 GHz (2 GHz). The transconductance of the de-
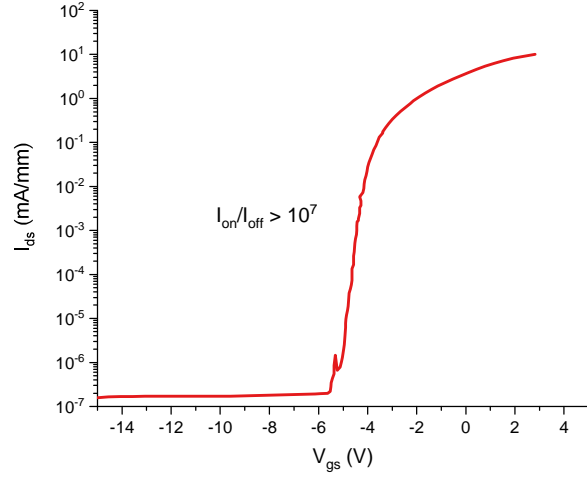


**Fig. 17.** Semi-log transfer characteristics measured at $V_{DS} = 30$ V of the FP MOSFET, adapted from [134].
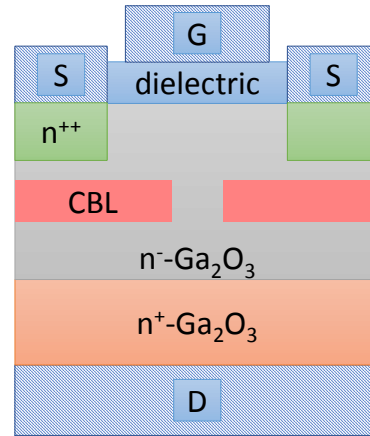


**Fig. 18.** Cross-section of vertical MOSFET with current blocking layer (CBL), adapted from [136].

vice and $I_{on}/I_{off}$ were 40 mS/mm and $10^8$. Mun *et al.* in ref. [134] manufactured a β-$Ga_2O_3$ MOSFET with a field electrode at the source contact and a breakdown voltage -2.32 kV (Fig. 17). This device was obtained by molecular beam epitaxy on an Fe-doped substrate. The $I_{on}/I_{off}$ ratio was $10^7$. The investigated dependence of the breakdown voltage from the distance between the drain and the gate turned out to be directly proportional. Liddy *et al.* in ref. [135] implemented a β-$Ga_2O_3$ MOSFET with refractory metals as contacts and a self-aligned gate. The resulting device has a transconductance of 35 mS/mm, a drain current density of 140 mA/mm and an $I_{on}/I_{off}$ of more than $10^8$, subthreshold slope - 121 mV/dec. Also, the authors suggested that changing the size of the gate contact would increase the transconductance to 60 mS/mm. Wong *et al.* in ref. [136] manufactured a vertical transistor on $Ga_2O_3$ with a current aperture obtained by Mg ion implantation (Fig. 18). The diffusion of Mg atoms led to a high leakage current between the drain and the source, due to which the characteristics of the device turned out to be lower than those obtained in

computer simulations. The transconductance of the device was 1.25 mS/mm with a drain displacement of 8 V. Later Wong *et al.* in ref. [137] showed an improvement in the transistor characteristics upon implantation of Si ions in the drain and source contacts region. The maximum drain current was 1.4 mA/mm when the $I_{on}/I_{off}$ ratio is $10^6$.

Researchers often resort to structural modifications to improve the device performance. For example, Ma *et al.* in ref. [138] investigated a MESFET with two asymmetric bases on β-Ga$_2$O$_3$ nanomembrane. The device characteristics: threshold voltage -57.7 V, The $I_{on}/I_{off}$ ratio $1.7 \cdot 10^8$, subthreshold slope - 470 mV/dec. Chabak *et al.* in ref. [139] grew a transistor with a buried gate by molecular beam epitaxy. The current from the drain is 40 mA/mm, $I_{on}/I_{off}$ is about $10^9$. The maximum breakdown voltage for the resulting devices is 505 V, the subthreshold slope is 200 mV/dec. Sasaki *et al.* in ref. [140] obtained a vertical trench MOSFET on a (001) Ga$_2$O$_3$ substrate by chloride-hydride gas-phase epitaxy. $I_{on}/I_{off}$ is about $10^3$, the switched-on resistance is 3.7 mΩ·cm². The device performed good static characteristics, however turn-off characteristics are negligible due to high leakage current.

A possible way to FETs modification is to study individual characteristics and the defects influence investigation. So, McGlone *et al.* in ref. [141] examined traps in the Si δ-doped β-Ga$_2$O$_3$ MESFET intermediate layer. Two traps with energies of -0.7 eV and -0.8 eV were found, which leads to threshold voltage and turn-on series resistance deterioration. The -0.8 eV level was attributed to defects associated with Fe, while -0.7 eV was attributed to the point defect of the β-Ga$_2$O$_3$ crystal. Polyakov *et al.* in ref. [142] investigated the levels of defects in a transistor on a β-Ga$_2$O$_3$ nanoplate. The need for passivation layers to prevent current collapse is shown, since the device characteristics are influenced by the molecules that are absorbed on the surface of the gallium oxide. The rate of $I_d$-$V_g$ change, the delay in the transistor opening and the current collapse in the pulsed mode depend on surface acceptors density with an energy of 1 eV. Reducing the acceptors concentration may improve the dynamic characteristics of the device. Wong *et al.* in ref. [143] examined the main charge carriers mobility in a MOSFET with a buffer layer that protects the channel from charge compensation by suppressing the Fe atoms diffusion and enhance the transistor electrical performance. When growth temperature increased from 560 to 650 °C, the leakage current through the buffer layer decreased $10^7$ times. The main negative effect of buffer insertion is parasitic conduction at the buffer/substrate heterointerface.

Different types of FET based on different gallium oxide polymorphs heterostructures were reported, but most common (or more investigated) type is MOSFET. For all types a vertical realization of transistor is more frequent due to easier fabrication. It was shown that the device structure should be modified (ion implanted aperture/trenches) to achieve theoretical breakdown electrical field value 8 MV/cm. The $I_{on}/I_{off}$ for all devices are in $10^6$-$10^{10}$ range, smaller values were obtained due to structural or interface defects. β-Ga$_2$O$_3$ high thermal stability provides FET steady operation with temperatures up to 250 °C.



**Fig. 19.** EPR spectrum of Co$^{2+}$ in β-Ga$_2$O$_3$ measured at 6 K with B‖a*, adapted from [145].

## 9. SPINTRONIC APPLICATIONS

Along with the electrical, thermal, and chemical properties, in recent years, much attention has been paid to the gallium oxide magnetic properties study for use in spintronic devices. Thus, a number of research groups have investigated the magnetic properties of various Ga$_2$O$_3$ polymorphic modifications.

Luan *et al.* in ref. [144] investigated the structural, elastic and electronic properties of the *â*-Ga$_2$O$_3$ crystal at pressures from 0 to 30 GPa. Calculations have shown that with pressure increasing, the band gap increases monotonically. It was also determined that the *a* lattice parameter compression occurs more easily than *b*, *c*. The calculated results of the change in the lattice constants are in agreement with the experimental results of X-ray structural analysis.

Stehr *et al.* in ref. [145] first measured the electron paramagnetic resonance spectra for Co$^{2+}$ and Cu$^{2+}$ in a β-Ga$_2$O$_3$ crystal (Fig. 19). It was shown that Co and Cu are present in the 2$^+$ state in the 3d7 and 3d9 configurations, respectively. Atoms with a large ionic radius preferably take the place of octahedral Ga in the crystal lattice.

Wang *et al.* in ref. [146] investigated the electronic structure and magnetic properties of β-Ga$_2$O$_3$ doped
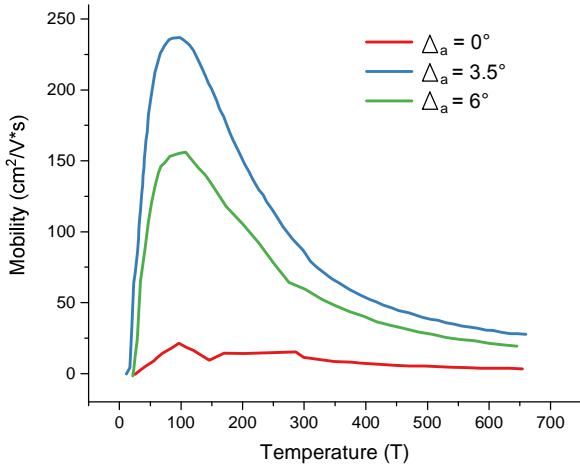
**Fig. 20.** Temperature dependent Hall measurements for the Si doped β-Ga$_2$O$_3$ thin films grown on c-plane sapphire substrates with different off angles toward <11$\overline{2}$0>, adapted from [151].

with Mn. Pure gallium oxide band structure and the effect of Mn atoms incorporation was studied. Thus, doping leads to the formation of additional bands, which reduces the gallium oxide band gap. A crystal turns out to have the most stable structure and ferromagnetism if Mn atoms replace only the sites of octahedral Ga in the crystal lattice. For such a case, the calculation shows a Curie temperature of 421 K.

Shi *et al.* in ref. [147] described the production of high quality CuGa$_2$O$_4$ layers by copper layer evaporation at 1050 °C. The obtained samples were studied on a diffractometer, the measurements results showed an epitaxial bond between the CuGa$_2$O$_4$ layer and the β-Ga$_2$O$_3$ (2$\overline{0}$1) substrate. The CuGa$_2$O$_4$ epitaxial layer (222) FWHM was 0.228°. The discrepancy in the lattice constants was 8.71%.

Hsieh *et al.* in ref. [148] got a metal-insulator-semiconductor (MIS) diode with a thin layer of α-Ga$_2$O$_3$ as an insulator. Gallium oxide was obtained by liquid-phase epitaxy and subsequent annealing at 400 °C. The manu-

factured Ni/α-Ga$_2$O$_3$/Si MIS diode has an $I_{on}/I_{off}$ ratio 100 times better than Ni/Si Schottky diode. Leakage current at -2 V bias was 1.07·10$^{-5}$ A/cm$^2$, breakdown voltage -166 V, barrier height 1.085 eV.

The results shown indicate the possibility of using gallium oxide to create spintronic devices - computer and track memory, spin transistors, and logic circuits. At the same time, the magnetic properties have not been fully investigated, and the topic remains relevant and requires further study.

## 10. OTHER DEVICES

Technological applications of gallium oxide in a number of areas are studied less intensively, but the results obtained allows to judge its prospects and high potential. For example, Kumar *et al.* in ref. [149] reported a brief review about the properties of gallium oxide nanostructures and nanowires. Also, applications of such nanotechnology was described.

Huang *et al.* in ref. [150] investigated the structural and photoelectric properties of â Ga$_2$O$_3$/SiC multilayers grown by molecular beam epitaxy on sapphire (0001) substrates. Several samples were obtained with different annealing conditions, all of them exhibit a photoelectric response to the 254 nm UV radiation. Additional annealing of the SiC layer affects its crystallinity and leads to a decrease in carrier concentration. In turn, the sensitivity to UV radiation completely depends on the annealing conditions of the Ga$_2$O$_3$ layer.

Rafique *et al.* in ref. [151] examined the heteroepitaxial growth of β-Ga$_2$O$_3$ on sapphire (0001) substrates with an off-axis angle of up to 10° in the <11-20> direction (Fig. 20). Thin films were obtained using chemical vapor deposition at low pressure. The crystal structure and surface quality, as well as the electrical conductivity, strongly depend on the angle of deflection relative to the substrate axis. Such substrates utilization led to a decrease in the FWHM and an increase of the Raman peaks intensity relative to the layers ob-
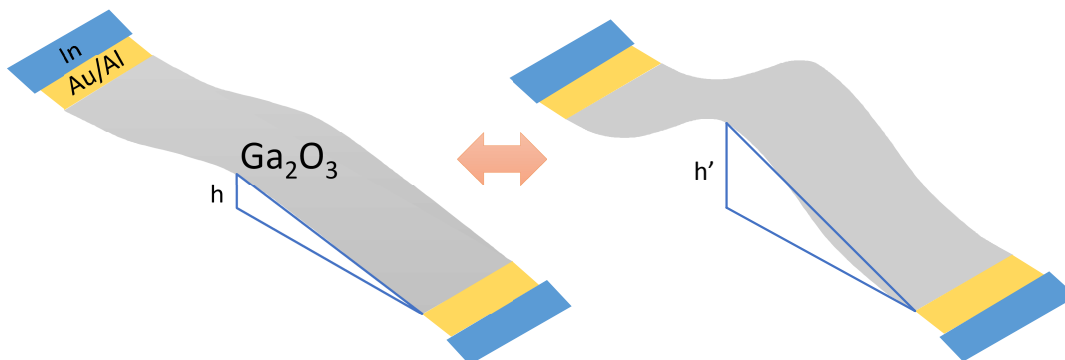


**Fig. 21.** Thermal actuator schematic, adapted from [154].

tained on flat substrates. The best performance was obtained with a substrate with a deflection of 6°.

Sun *et al.* in ref. [152] conducted the energy bands study of the β-Ga$_2$O$_3$/AlN heterojunction. A gallium oxide layer of no more than 2 nm was deposited on AlN/sapphire by pulsed laser deposition. For the obtained heterojunction, the shifts of the valence and conduction bands were measured, which amounted to -0.55 and -1.75 eV, respectively.

Rodriguez *et al.* in ref. [153] used α-Ga$_2$O$_3$ as a photocatalyst for the decomposition of malachite green. The study of gallium oxide on a diffractometer after the catalytic reaction showed no phase transition in the material.

Peres *et al.* in ref. [154] showed the first Ga$_2$O$_3$-based temperature activated mechanical actuator (Fig. 21). The device works on the principle of thermal expansion of the material during self-heating while passing current through the plate. The maximum value that the drive has risen is 42.38 microns.

Gallium oxide is a promising material, but the current research results are still insufficient realize its full potential. Thus, the absence of a normal substrate for gallium oxide makes it necessary to investigate the ability of growing epitaxial layers on materials with which the lattice constant is very different. Also, the applications of Ga$_2$O$_3$ as a mechanical micro-piston or as a photocatalyst are also interesting to consider. Further studies of such a material as gallium oxide will allow to understand its potential more accurately for creating various devices and, probably, will make it possible to achieve its maximum theoretical characteristics.

## 11. SUMMARY AND CONCLUSIONS

The review considers both the gallium oxide main application areas and areas that are at the initial stage of development and require additional large-scale investigations to study the proposed solutions effectiveness.

The unique Ga$_2$O$_3$ physical properties allow it to remain one of the most interesting and promising wide band gap semiconductors for quite a long time. At the moment, six of its polymorphic modifications have been investigated, among which the β-Ga$_2$O$_3$ attracts researchers special attention due to its high stability. The increased interest is confirmed by a large number of reports devoted to both the study of the β-Ga$_2$O$_3$ growth technology and â-Ga$_2$O$_3$ based device manufacturing.

The wide band gap, high breakdown voltage, and sufficiently high mobility determine the gallium oxide main application areas: solar-blind photodetectors, power rectifiers and transistors, resistive memory devices. The most significant results have been shown in these areas to date. Meanwhile, a fairly large number of reports are devoted to the Ga$_2$O$_3$ luminescent properties investigation, and the development of multi-colored phosphors based on it, as well as the study of the magnetic properties in the case of doping with various metals for spintronic devices. The poorly studied application areas described at the separated review section are no less interesting in the future development of gallium oxide technology.

## ACKNOWLEDGEMENTS

## REFERENCES

[1] NSM Archive - Physical Properties of Semiconductors, (n.d.). http://www.ioffe.ru/SVA/NSM/Semicond/ (accessed September 15, 2021).

[2] R. Roy, V.G. Hill and E.F. Osborn, *Polymorphism of Ga$_2$O$_3$ and the System Ga$_2$O$_3$-H$_2$O*, J. Am. Chem. Soc., 1952, vol. 74, pp. 719–722. https://doi.org/10.1021/ja01123a039

[3] H.Y. Playford, A.C. Hannon, E.R. Barney and R.I. Walton, *Structures of Uncharacterised Polymorphs of Gallium Oxide from Total Neutron Diffraction*, Chem. - A Eur. J., 2013, vol. 19, no. 8, pp. 2803–2813. https://doi.org/10.1002/chem.201203359

[4] S.I. Stepanov, V.I. Nikolaev, V.E. Bougrov and A.E. Romanov, *Gallium oxide: Properties and applications - A review*, Rev. Adv. Mater. Sci., 2016, vol. 44, no. 1, pp. 63–86. https://www.ipme.ru/e-journals/RAMS/no_14416/06_14416_stepanov.pdf

[5] H. He, M.A. Blanco and R. Pandey, *Electronic and thermodynamic properties of β-Ga$_2$O$_3$*, Appl. Phys. Lett., 2006, vol. 88, art. 261904. https://doi.org/10.1063/1.2218046

[6] S. Yoshioka, H. Hayashi, A. Kuwabara, F. Oba, K. Matsunaga and I. Tanaka, *Structures and energetics of Ga$_2$O$_3$ polymorphs*, J. Phys. Condens. Matter., 2007, vol. 19, art. 346211. https://doi.org/10.1088/0953-8984/19/34/346211

[7] N.D. Cuong, Y.W. Park and S.G. Yoon, *Microstructural and electrical properties of Ga2O3 nanowires grown at various temperatures by vapor–liquid–solid technique*, Sensors Actuators B Chem., 2009, vol. 140, no. 1, pp. 240–244. https://doi.org/10.1016/j.snb.2009.04.020

[8] A. Fiedler, R. Schewski, Z. Galazka and K. Irmscher, *Static Dielectric Constant of β-Ga$_2$O$_3$ Perpendicular to the Principal Planes (100), (010), and (001)*, ECS J. Solid State Sci. Technol.,

2019, vol. 8, no. 7, pp. Q3083–Q3085. https://doi.org/10.1149/2.0201907jss

[9] S.J. Pearton, J. Yang, P.H. Cary, F. Ren, J. Kim, M.J. Tadjer and M.A. Mastro, *A review of $Ga_2O_3$ materials, processing, and devices*, Appl. Phys. Rev., 2018, vol. 5, pp. 0–56. https://doi.org/10.1063/1.5006941

[10] M.J. Tadjer, F. Alema, A. Osinsky, M.A. Mastro, N. Nepal, J.M. Woodward, R.L. Myers-Ward, E.R. Glaser, J.A. Freitas, A.G. Jacobs, J.C. Gallagher, A.L. Mock, D.J. Pennachio, J. Hajzus, M. Ebrish, T.J. Anderson, K.D. Hobart, J.K. Hite and C.R. Eddy Jr., *Characterization of β-$Ga_2O_3$ homoepitaxial films and MOSFETs grown by MOCVD at high growth rates*, J. Phys. D. Appl. Phys., 2012, vol. 54, art. 034005. https://doi.org/10.1088/1361-6463/abbc96

[11] M. Higashiwaki, K. Sasaki, A. Kuramata, T. Masui and S. Yamakoshi, *Gallium oxide ($Ga_2O_3$) metal-semiconductor field-effect transistors on single-crystal β-$Ga_2O_3$ (010) substrates*, Appl. Phys. Lett., 2012, vol. 100, pp. 1–4. https://doi.org/10.1063/1.3674287

[12] M. Yan-Mei, C. Hai-Yong, Y. Kai-Feng, L. Min, C. Qi-Liang, L. Jing and Z. Guang-Tian, *High-Pressure and High-Temperature Behaviour of Gallium Oxide*, Chinese Phys. Lett., 2008, vol. 25, pp. 1603–1605. https://doi.org/10.1088/0256-307X/25/5/022

[13] A. Kuramata, K. Koshi, S. Watanabe, Y. Yamaoka, T. Masui and S. Yamakoshi, *High-quality β-$Ga_2O_3$ single crystals grown by edge-defined film-fed growth*, Jpn. J. Appl. Phys., 2016, vol. 55, no. 12, art. 1202A2. https://doi.org/10.7567/JJAP.55.1202A2

[14] K. Kaneko, T. Nomura, I. Kakeya and S. Fujita, *Fabrication of Highly Crystalline Corundum-Structured α-$(Ga_{1-x}Fe_x)_2O_3$ Alloy Thin Films on Sapphire Substrates*, Appl. Phys. Express., 2009, vol. 2, no. 7, art. 075501. https://doi.org/10.1143/APEX.2.075501

[15] H. Hayashi, R. Huang, H. Ikeno, F. Oba, S. Yoshioka, I. Tanaka and S. Sonoda, *Room temperature ferromagnetism in Mn-doped γ-$Ga_2O_3$ with spinel structure*, Appl. Phys. Lett., 2006, vol. 89, art. 181903. https://doi.org/10.1063/1.2369541

[16] M.B. Maccioni and V. Fiorentini, Phase diagram and polarization of stable phases of $(Ga_{1-x}In_x)_2O_3$, Appl. Phys. Express., 2016, vol. 9, no. 4, art. 041102. https://doi.org/10.7567/APEX.9.041102

[17] X. Xia, Y. Chen, Q. Feng, H. Liang, P. Tao, M. Xu and G. Du, *Hexagonal phase-pure wide band gap ε-$Ga_2O_3$ films grown on 6H-SiC substrates*

by *metal organic chemical vapor deposition*, Appl. Phys. Lett., 2016, vol. 108, no. 20, art. 202103. https://doi.org/10.1063/1.4950867

[18] M.B. Sahariah and C.Y. Kadolkar, *Short range potential parameters and electronic polarizabilities of β-$Ga_2O_3$*, J. Phys. Condens. Matter., 2007, vol. 19, art. 156215. https://doi.org/10.1088/0953-8984/19/15/156215

[19] J.B. Varley, J.R. Weber, A. Janotti and C.G. Van de Walle, *Oxygen vacancies and donor impurities in β-$Ga_2O_3$*, Appl. Phys. Lett., 2010, vol. 97, art. 142106. https://doi.org/10.1063/1.3499306

[20] D.A. Bauman, A.I. Borodkin, A.A. Petrenko, D.I. Panov, A.V. Kremleva, V.A. Spiridonov, D.A. Zakgeim, M.V. Silnikov, M.A. Odnoblyudov, A.E. Romanov and V.E. Bougrov, *On improving the radiation resistance of gallium oxide for space applications*, Acta Astronaut., 2021, vol. 180, pp. 125–129. https://doi.org/10.1016/j.actaastro.2020.12.010

[21] M.A. Mastro, A. Kuramata, J. Calkins, J. Kim, F. Ren and S.J. Pearton, *Perspective— Opportunities and Future Directions for $Ga_2O_3$*, ECS J. Solid State Sci. Technol., 2017, vol. 6, no. 7, pp. P356–P359. https://doi.org/10.1149/2.0031707jss

[22] D. Guo, Q. Guo, Z. Chen, Z. Wu, P. Li and W. Tang, *Review of $Ga_2O_3$-based optoelectronic devices*, Mater. Today Phys., 2019, vol. 11, art. 100157. https://doi.org/10.1016/j.mtphys.2019.100157

[23] M. Bartic, M. Ogita, M. Isai, C.L. Baban and H. Suzuki, *Oxygen sensing properties at high temperatures of Â-$Ga_2O_3$ thin films deposited by the chemical solution deposition method*, J. Appl. Phys., 2007, vol. 102, no. 2, art. 023709. https://doi.org/10.1063/1.2756085

[24] M. Bartic, Y. Toyoda, C.I. Baban and M. Ogita, *Oxygen sensitivity in gallium oxide thin films and single crystals at high temperatures*, Japanese J. Appl. Physics, Part 1 Regul. Pap. Short Notes Rev. Pap., 2006, vol. 45, no 6R, pp.5186–5188. https://doi.org/10.1143/JJAP.45.5186

[25] M. Ogita, K. Higo, Y. Nakanishi and Y. Hatanaka, *$Ga_2O_3$ thin film for oxygen sensor at high temperature*, Appl. Surf. Sci., 2001, vol. 175-176, pp. 721–725. https://doi.org/10.1016/S0169-4332(01)00080-0

[26] C. Baban, Y. Toyoda and M. Ogita, *Oxygen sensing at high temperatures using $Ga_2O_3$ films*, Thin Solid Films., 2005, vol. 484, no. 1-2, pp. 369–373. https://doi.org/10.1016/j.tsf.2005.03.001

[27] Y. Li, A. Trinchi, W. Wlodarski, K. Galatsis and K. Kalantar-Zadeh, I*nvestigation of the oxygen gas sensing performance of Ga₂O₃ thin films with different dopants*, Sensors Actuators, B Chem., 2003, vol. 93, no. 1-3, pp. 431–434. https://doi.org/10.1016/S0925-4005(03)00171-0

[28] A. Trinchi, S. Kaciulis, L. Pandolfi, M.K. Ghantasala, Y.X. Li, W. Wlodarski, S. Viticoli, E. Comini and G. Sberveglieri, *Characterization of Ga₂O₃ based MRISiC hydrogen gas sensors*, Sensors Actuators B Chem., 2004, vol. 103, no. 1-2, pp. 129–135. https://doi.org/10.1016/j.snb.2004.04.112

[29] J. Frank, M. Fleischer, H. Meixner and A. Feltz, *Enhancement of sensitivity and conductivity of semiconducting Ga₂O₃ gas sensors by doping with SnO₂*, Sensors Actuators B Chem., 1998, vol. 49, no. 1-2, pp. 110–114. https://doi.org/10.1016/S0925-4005(98)00094-X

[30] V. Balasubramani, A.N. Ahamed, S. Chandraleka, K.K. Kumar, M.R. Kuppusamy and T.M. Sridhar, *Highly Sensitive and Selective H₂S Gas Sensor Fabricated with* β*-Ga₂O₃/rGO*, ECS J. Solid State Sci. Technol., 2020, vol. 9, no. 5, art. 055009. https://doi.org/10.1149/2162-8777/ab9a18

[31] R. Pohle, E. Weisbrod and H. Hedler, *Enhancement of MEMS-based Ga₂O₃ Gas Sensors by Surface Modifications*, Procedia Eng., 2016, vol. 168, pp. 211–215. https://doi.org/10.1016/j.proeng.2016.11.164

[32] Q.C. Bui, L. Largeau, M. Morassi, N. Jegenyes, O. Mauguin, L. Travers, X. Lafosse, C. Dupuis, J.C. Harmand, M. Tchernycheva and N. Gogneau, *GaN/Ga₂O₃ core/shell nanowires growth: Towards high response gas sensors*, Appl. Sci., 2019, vol. 9, no. 17, pp. 1–14. https://doi.org/10.3390/app9173528

[33] Z. Liu, T. Yamazaki, Y. Shen, T. Kikuta, N. Nakatani and Y. Li, *O₂ and CO sensing of Ga₂O₃ multiple nanowire gas sensors*, Sensors Actuators B Chem., 2008, vol. 129, pp. 666–670. https://doi.org/10.1016/j.snb.2007.09.055

[34] C. Jin, S. Park, H. Kim and C. Lee, *Ultrasensitive multiple networked Ga₂O₃-core/ZnO- shell nanorod gas sensors*, Sensors Actuators B Chem., 2012, vol. 161, no. 1, pp. 223–228. https://doi.org/10.1016/j.snb.2011.10.023

[35] L. Mazeina, F.K. Perkins, V.M. Bermudez, S.P. Arnold and S.M. Prokes, *Functionalized Ga₂O₃ nanowires as active material in room temperature capacitance-based gas sensors*, Langmuir, 2010, vol. 26, no. 16, pp. 13722–13726. https://doi.org/10.1021/la101760k

[36] A. Afzal, β-*Ga₂O₃ nanowires and thin films for metal oxide semiconductor gas sensors: Sensing mechanisms and performance enhancement strategies*, J. Mater., 2019, vol. 5, no. 1, pp. 542–557. https://doi.org/10.1016/j.jmat.2019.08.003

[37] Y.K. Frodason, K.M. Johansen, L. Vines and J.B. Varley, *Self-trapped hole and impurity-related broad luminescence in* β-*Ga₂O₃*, J. Appl. Phys., 2020, vol. 127, no. 7,. art. 075701. https://doi.org/10.1063/1.5140742

[38] H. Tang, N. He, Z. Zhu, M. Gu, B. Liu, J. Xu, M. Xu, L. Chen, J. Liu and X. Ouyang, *Temperature-dependence of X-ray excited luminescence of* β-*Ga₂O₃ single crystals*, Appl. Phys. Lett., 2019, vol. 115, no. 7, art. 071904. https://doi.org/10.1063/1.5110535

[39] X. Yu, H. Cui, M. Zhu, Z. Xia and Q. Sai, *Influence of annealing treatment on the luminescent properties of Ta:* β-*Ga₂O₃ single crystal*, Chinese Phys. B., 2019, vol. 28, no. 7, art. 077801. https://doi.org/10.1088/1674-1056/28/7/077801

[40] T.T. Huynh, E. Chikoidze, C.P. Irvine, M. Zakria, Y. Dumont, F.H. Teherani, E. V Sandana, P. Bove, D.J. Rogers, M.R. Phillips and C. Ton-That, *Red luminescence in H-doped* β-*Ga₂O₃*, Phys. Rev. Mat., 2020, vol. 4, art. 085201. https://doi.org/10.1103/PhysRevMaterials.4.085201

[41] A. Luchechko, V. Vasyltsiv, L. Kostyk, O. Tsvetkova and B. Pavlyk, *Thermally stimulated luminescence and conductivity of* β-*Ga₂O₃ crystals*, J. Nano- Electron. Phys., 2019, vol. 11, no. 3, pp. 1–7. https://doi.org/10.21272/jnep.11(3).03035

[42] A.Y. Polyakov, N.B. Smirnov, I. V. Schemerov, A.V. Chernykh, E.B. Yakimov, A.I. Kochkova, A.N. Tereshchenko and S.J. Pearton, Electrical Properties, *Deep Levels and Luminescence Related to Fe in Bulk Semi-Insulating* β-*Ga₂O₃ Doped with Fe*, ECS J. Solid State Sci. Technol., 2019, vol. 8, no. 7, pp. Q3091–Q3096. https://doi.org/10.1149/2.0171907jss

[43] A.Y. Polyakov, N.B. Smirnov, I. V. Shchemerov, E.B. Yakimov, S.J. Pearton, F. Ren, A. V. Chernykh, D. Gogova and A.I. Kochkova, *Electrical Properties, Deep Trap and Luminescence Spectra in Semi-Insulating, Czochralski* β-*Ga₂O₃ (Mg)*, ECS J. Solid State Sci. Technol., 2019, vol. 8, no. 7, pp. Q3019–Q3023. https://doi.org/10.1149/2.0041907jss

[44] Z. Gao, L. Yu, X. Man, J. Zhong, Q. Guo and Y. Zou, T*he structure and luminescence properties of Mn²⁺/Eu²⁺/Er³⁺-doped MgO-Ga₂O₃-SiO₂ glasses and glass-ceramics*, Luminescence,

2019, vol. 34, no. 8, pp. 830–837. https://doi.org/10.1002/bio.3678

[45] J. Ueda, A. Hashimoto and S. Tanabe, *Orange Persistent Luminescence and Photodarkening Related to Paramagnetic Defects of Nondoped CaO-Ga$_2$O$_3$-GeO$_2$ Glass*, J. Phys. Chem. C., 2019, vol. 123, no. 49, pp. 29946–29953. https://doi.org/10.1021/acs.jpcc.9b07638

[46] J. Jiang, J. Zhang, J. Li and D. Xu, *Red-light emission of Li-doped Ga$_2$O$_3$ one-dimensional nanostructures and the luminescence mechanism*, Chem. Phys. Lett., 2019, vol. 719, pp. 8–11. https://doi.org/10.1016/j.cplett.2019.01.003

[47] J. Jiang, J. Zhang and Z. Song, Influence of Zn doping on the morphology and luminescence of Ga$_2$O$_3$ low-dimensional nanostructures, J. Lumin., 2020, vol. 221, art. 117048. https://doi.org/10.1016/j.jlumin.2020.117048

[48] J. Yang, F. Ren, M. Tadjer, S.J. Pearton and A. Kuramata, *2300V Reverse Breakdown Voltage Ga$_2$O$_3$ Schottky Rectifiers*, ECS J. Solid State Sci. Technol., 2018, vol. 7, pp. Q92–Q96. https://doi.org/10.1149/2.0241805jss

[49] C. Hou, R.A. Makin, K.R. York, S.M. Durbin, J.I. Scott, R.M. Gazoni, R.J. Reeves and M.W. Allen, *High-temperature (350 °C) oxidized iridium Schottky contacts on β-Ga$_2$O$_3$*, Appl. Phys. Lett., 2019, vol. 114, art. 233503. https://doi.org/10.1063/1.5099126

[50] E. Swinnich, M.N. Hasan, K. Zeng, Y. Dove, U. Singisetti, B. Mazumder and J.H. Seo, *Flexible β-Ga$_2$O$_3$ Nanomembrane Schottky Barrier Diodes*, Adv. Electron. Mater., 2019, vol. 5, no. 3, art. 1800714. https://doi.org/10.1002/aelm.201800714

[51] K. Sasaki, A. Kuramata, T. Masui, E.G. Víllora, K. Shimamura and S. Yamakoshi, *Device-quality β-Ga$_2$O$_3$ epitaxial films fabricated by ozone molecular beam epitaxy*, Appl. Phys. Express., 2012, vol. 5, no. 3, pp. 5–8. https://doi.org/10.1143/APEX.5.035502

[52] T. Harada, S. Ito and A. Tsukazaki, *Electric dipole effect in PdCoO$_2$/β-Ga$_2$O$_3$ Schottky diodes for high-temperature operation*, Sci. Adv., 2019, vol. 5, no. 10, pp. 1–7. https://doi.org/10.1126/sciadv.aax5733

[53] X. Huang, F. Liao, L. Li, X. Liang, Q. Liu, C. Zhang and X. Hu, *3.4 kV Breakdown Voltage Ga$_2$O$_3$ Trench Schottky Diode with Optimized Trench Corner Radius*, ECS J. Solid State Sci. Technol., 2020, vol. 9, no. 4, art. 045012. https://doi.org/10.1149/2162-8777/ab8b4a

[54] S. Müller, L. Thyen, D. Splith, A. Reinhardt, H. von Wenckstern and M. Grundmann, *High-Quality Schottky Barrier Diodes on β-Gallium Oxide Thin Films on Glass Substrate*, ECS J. Solid State Sci. Technol., 2019, vol. 8, pp. Q3126–Q3132. https://doi.org/10.1149/2.0241907jss

[55] E. Farzana, Z. Zhang, P.K. Paul, A.R. Arehart and S.A. Ringel, *Influence of metal choice on (010) β-Ga$_2$O$_3$ Schottky diode properties*, Appl. Phys. Lett., 2017, vol. 110, art. 202102. https://doi.org/10.1063/1.4983610

[56] K. Jiang, L.A.M. Lyle, E. Favela, D. Moody, T. Lin, K.K. Das, A. Popp, Z. Galazka, G. Wagner and L.M. Porter, *Electrical Properties of (100) β-Ga$_2$O$_3$ Schottky Diodes with Four Different Metals*, ECS Trans., 2019, vol. 92, no. 7, pp. 71–78. https://doi.org/10.1149/09207.0071ecst

[57] M. Xian, C. Fares, F. Ren, B.P. Gila, Y.-T. Chen, Y.-T. Liao, M. Tadjer and S.J. Pearton, *Effect of thermal annealing for W/β-Ga$_2$O$_3$ Schottky diodes up to 600 °C*, J. Vac. Sci. Technol. B., 2019, vol. 37, art. 061201. https://doi.org/10.1116/1.5125006

[58] C. Fares, F. Ren and S.J. Pearton, *Temperature-Dependent Electrical Characteristics of β-Ga$_2$O$_3$ Diodes with W Schottky Contacts up to 500 °C*, ECS J. Solid State Sci. Technol., 2019, vol. 8, pp. Q3007–Q3012. https://doi.org/10.1149/2.0011907jss

[59] P.R.S. Reddy, V. Janardhanam, K.H. Shim, V.R. Reddy, S.N. Lee, S.J. Park and C.J. Choi, *Temperature-dependent Schottky barrier parameters of Ni/Au on n-type (001) β-Ga$_2$O$_3$ Schottky barrier diode*, Vacuum, 2020, vol. 171, art. 109012. https://doi.org/10.1016/j.vacuum.2019.109012

[60] Z.A. Jian, S. Mohanty and E. Ahmadi, *Temperature-dependent current-voltage characteristics of β-Ga$_2$O$_3$ trench Schottky barrier diodes*, Appl. Phys. Lett., 2020, vol. 116, pp. 3–8. https://doi.org/10.1063/5.0002520

[61] W. Li, D. Saraswat, Y. Long, K. Nomoto, D. Jena and H.G. Xing, *Near-ideal reverse leakage current and practical maximum electric field in β-Ga$_2$O$_3$ Schottky barrier diodes*, Appl. Phys. Lett., 2020, vol. 116, art. 192101. https://doi.org/10.1063/5.0007715

[62] M. Kasu, K. Hanada, T. Moribayashi, A. Hashiguchi, T. Oshima, T. Oishi, K. Koshi, K. Sasaki, A. Kuramata and O. Ueda, *Relationship between crystal defects and leakage current in β-Ga$_2$O$_3$ Schottky barrier diodes*, Jpn. J. Appl. Phys., 2016, vol. 55, no. 12, art. 1202BB. https://doi.org/10.7567/JJAP.55.1202BB

[63] M. Kasu, T. Oshima, K. Hanada, T. Moribayashi, A. Hashiguchi, T. Oishi, K. Koshi, K. Sasaki, A. Kuramata and O. Ueda, C*rystal defects observed by the etch-pit method and their effects on Schottky-barrier-diode characteristics on (201) β-Ga$_2$O$_3$*, Jpn. J. Appl. Phys., 2017, vol. 56, no. 9, art. 091101. https://doi.org/10.7567/JJAP.56.091101

[64] T. Oshima, A. Hashiguchi, T. Moribayashi, K. Koshi, K. Sasaki, A. Kuramata, O. Ueda, T. Oishi and M. Kasu, *Electrical properties of Schottky barrier diodes fabricated on (001) β-Ga$_2$O$_3$ substrates with crystal defects*, Jpn. J. Appl. Phys., 2017, vol. 56, no. 8, art. 086501. https://doi.org/10.7567/JJAP.56.086501

[65] D. Khan, D. Gajula, S. Okur, G.S. Tompa and G. Koley, β-*Ga$_2$O$_3$ Thin Film Based Lateral and Vertical Schottky Barrier Diode*, ECS J. Solid State Sci. Technol., 2019, vol. 8, pp. Q106–Q110. https://doi.org/10.1149/2.0211906jss

[66] R. Lingaparthi, K. Sasaki, Q.T. Thieu, A. Takatsuka, F. Otsuka, S. Yamakoshi and A. Kuramata, *Surface related tunneling leakage in β-Ga$_2$O$_3$ (001) vertical Schottky barrier diodes*, Appl. Phys. Express., 2019, vol. 12, no. 7, art. 074008. https://doi.org/10.7567/1882-0786/ab2824

[67] S. Modak, L. Chernyak, S. Khodorov, I. Lubomirsky, J. Yang, F. Ren and S.J. Pearton, *Impact of Electron Injection and Temperature on Minority Carrier Transport in Alpha-Irradiated β-Ga$_2$O$_3$ Schottky Rectifiers*, ECS J. Solid State Sci. Technol., 2019, vol. 8, no. 7, pp. Q3050–Q3053. https://doi.org/10.1149/2.0101907jss

[68] K. Konishi, K. Goto, H. Murakami, Y. Kumagai, A. Kuramata, S. Yamakoshi and M. Higashiwaki, *1-kV vertical Ga$_2$O$_3$ field-plated Schottky barrier diodes*, Appl. Phys. Lett., 2017, vol. 110, art. 103506. https://doi.org/10.1063/1.4977857

[69] X. Lu, X. Zhang, H. Jiang, X. Zou, K.M. Lau and G. Wang, *Vertical β-Ga$_2$O$_3$ Schottky Barrier Diodes with Enhanced Breakdown Voltage and High Switching Performance*, Phys. Status Solidi Appl. Mater. Sci., 2020, vol. 217, no. 3, art. 1900497. https://doi.org/10.1002/pssa.201900497

[70] S. Luan, L. Dong, X. Ma and R. Jia, *The further investigation of N-doped β-Ga$_2$O$_3$ thin films with native defects for Schottky-barrier diode*, J. Alloys Compd.,2020, vol. 812, no. 5, art. 152026. https://doi.org/10.1016/j.jallcom.2019.152026

[71] X. Lu, L. Zhou, L. Chen, X. Ouyang, H. Tang, B. Liu and J. Xu, *X-ray Detection Performance of Vertical Schottky Photodiodes Based on a Bulk β-Ga$_2$O$_3$ Substrate Grown by an EFG Method*,

ECS J. Solid State Sci. Technol., 2019, vol. 8, no. 7, pp. Q3046–Q3049. https://doi.org/10.1149/2.0071907jss

[72] L. Zhou, X. Lu, L. Chen, X. Ouyang, B. Liu, J. Xu and H. Tang, *Leakage Current by Poole–Frenkel Emission in Pt Schottky Contacts on () β-Ga$_2$O$_3$ Grown by Edge-Defined Film-Fed Growth*, ECS J. Solid State Sci. Technol., 2019, vol. 8, no. 7, pp. Q3054–Q3057. https://doi.org/10.1149/2.0111907jss

[73] P.E. Raad, P.L. Komarov, M.J. Tadjer, J. Yang, F. Ren, S.J. Pearton and A. Kuramata, *Thermoreflectance Temperature Mapping of Ga$_2$O$_3$ Schottky Barrier Diodes*, ECS Trans., 2019, vol. 89, no. 5, pp. 3-7. https://doi.org/10.1149/08905.0003ecst

[74] M. Oda, R. Tokuda, H. Kambara, T. Tanikawa, T. Sasaki and T. Hitora, *Schottky barrier diodes of corundum-structured gallium oxide showing on-resistance of 0.1mωcm$^2$ grown by MIST EPITAXY®*, Appl. Phys. Express., 2016, vol. 9, no. 2, art. 021101. https://doi.org/10.7567/APEX.9.021101

[75] J. Yang, S. Ahn, F. Ren, S.J. Pearton, S. Jang and A. Kuramata, *High breakdown voltage (-201) β-Ga$_2$O$_3$ Schottky rectifiers*, IEEE Electron Device Lett., 2017, vol. 38, no. 7, pp. 906–909. https://doi.org/10.1109/LED.2017.2703609

[76] C. Zhou, Q. Ai, X. Chen, X. Gao, K. Liu and D. Shen, *Ultraviolet photodetectors based on wide bandgap oxide semiconductor films*, Chinese Phys. B., 2019, vol. 28, no. 4, art. 048503. https://doi.org/10.1088/1674-1056/28/4/048503

[77] Y. Qin, S. Long, H. Dong, Q. He, G. Jian, Y. Zhang, X. Hou, P. Tan, Z. Zhang, H. Lv, Q. Liu and M. Liu, *Review of deep ultraviolet photodetector based on gallium oxide*, Chinese Phys. B., 2019, vol. 28, no. 1, art. 018501. https://doi.org/10.1088/1674-1056/28/1/018501

[78] M. Pavesi, F. Fabbri, F. Boschi, G. Piacentini, A. Baraldi, M. Bosi, E. Gombia, A. Parisini and R. Fornari, *ε-Ga$_2$O$_3$ epilayers as a material for solar-blind UV photodetectors*, Mater. Chem. Phys., 2018, vol. 205, pp. 502–507. https://doi.org/10.1016/j.matchemphys.2017.11.023

[79] D. Guo, Z. Wu, P. Li, Y. An, H. Liu, X. Guo, H. Yan, G. Wang, C. Sun, L. Li and W. Tang, *Fabrication of β-Ga$_2$O$_3$ thin films and solar-blind photodetectors by laser MBE technology*, Opt. Mater. Express., 2014, vol. 4, no. 5, pp. 1067-1076. https://doi.org/10.1364/ome.4.001067

[80] Y.F. Zhang, X.H. Chen, Y. Xu, F.F. Ren, S.L. Gu, R. Zhang, Y.D. Zheng and J.D. Ye, *Transition of photoconductive and photovoltaic operation*

*modes in amorphous Ga₂O₃-based solar-blind detectors tuned by oxygen vacancies*, Chinese Phys. B., 2019, vol. 28, no. 2, art. 028501. https://doi.org/10.1088/1674-1056/28/2/028501

[81] X. Chen, K. Liu, Z. Zhang, C. Wang, B. Li, H. Zhao, D. Zhao and D. Shen, *Self-Powered Solar-Blind Photodetector with Fast Response Based on Au/β-Ga₂O₃ Nanowires Array Film Schottky Junction*, ACS Appl. Mater. Interfaces., 2016, vol. 8, no. 6, pp. 4185–4191. https://doi.org/10.1021/acsami.5b11956

[82] D.Y. Guo, K. Chen, S.L. Wang, F.M. Wu, A.P. Liu, C.R. Li, P.G. Li, C.K. Tan and W.H. Tang, *Self-Powered Solar-Blind Photodetectors Based on α/β Phase Junction of Ga₂O₃*, Phys. Rev. Appl., 2020, vol. 13, art. 024051. https://doi.org/10.1103/PhysRevApplied.13.024051

[83] R. Suzuki, S. Nakagomi, Y. Kokubun, N. Arai and S. Ohira, *Enhancement of responsivity in solar-blind β-Ga₂O₃ photodiodes with a Au Schottky contact fabricated on single crystal substrates by annealing*, Appl. Phys. Lett., 2009, vol. 94, no. 22, art. 222102. https://doi.org/10.1063/1.3147197

[84] S. Nakagomi, T. Momo, S. Takahashi and Y. Kokubun, *Deep ultraviolet photodiodes based on β-Ga₂O₃/SiC heterojunction*, Appl. Phys. Lett., 2013, vol. 103, no. 7, art. 072105. https://doi.org/10.1063/1.4818620

[85] W.Y. Kong, G.A. Wu, K.Y. Wang, T.F. Zhang, Y.F. Zou, D.D. Wang and L.B. Luo, G*raphene-β-Ga₂O₃ Heterojunction for Highly Sensitive Deep UV Photodetector Application*, Adv. Mater., 2016, vol. 28, no. 48, pp. 10725–10731. https://doi.org/10.1002/adma.201604049

[86] X.H. Chen, Y.T. Chen, F.F. Ren, S.L. Gu, H.H. Tan, C. Jagadish and J.D. Ye, *Band alignment and band bending at β-Ga₂O₃/ZnO n-n isotype hetero-interface*, Appl. Phys. Lett., 2019, vol. 115, no. 20, art. 202101. https://doi.org/10.1063/1.5126325

[87] M. Chen, J. Ma, P. Li, H. Xu and Y. Liu, *Zero-biased deep ultraviolet photodetectors based on graphene/cleaved (100) Ga₂O₃ heterojunction*, Opt. Express, 2019, vol. 27, no. 6, pp. 8717-8726. https://doi.org/10.1364/oe.27.008717

[88] Y.H. An, D.Y. Guo, S.Y. Li, Z.P. Wu, Y.Q. Huang, P.G. Li, L.H. Li and W.H. Tang, *Influence of oxygen vacancies on the photoresponse of β-Ga₂O₃/SiC n-n type heterojunctions*, J. Phys. D. Appl. Phys., 2016, vol. 49, no. 28, art. 285111. https://doi.org/10.1088/0022-3727/49/28/285111

[89] F. Alema, B. Hertog, P. Mukhopadhyay, Y. Zhang, A. Mauze, A. Osinsky, W. V. Schoenfeld, J.S. Speck and T. Vogt, *Solar blind Schottky photodiode based on an MOCVD-grown homoepitaxial β-Ga₂O₃ thin film*, APL Mater., 2019, vol. 7, art. 022527. https://doi.org/10.1063/1.5064471

[90] T. Oshima, T. Okuno, N. Arai, N. Suzuki, S. Ohira and S. Fujita, *Vertical solar-blind deep-ultraviolet schottky photodetectors based on β-Ga₂O₃ substrates*, Appl. Phys. Express, 2008, vol. 1, no. 1, art. 011202. https://doi.org/10.1143/APEX.1.011202

[91] S. Cui, Z. Mei, Y. Zhang, H. Liang and X. Du, *Room-Temperature Fabricated Amorphous Ga₂O₃ High-Response-Speed Solar-Blind Photodetector on Rigid and Flexible Substrates*, Adv. Opt. Mater., 2017, vol. 5, no. 19, art. 1700454. https://doi.org/10.1002/adom.201700454

[92] W. Tian, C. Zhi, T. Zhai, S. Chen, X. Wang, M. Liao, D. Golberg and Y. Bando, *In-doped Ga₂O₃ nanobelt based photodetector with high sensitivity and wide-range photoresponse*, J. Mater. Chem., 2012, vol. 22, pp. 17984–17991. https://doi.org/10.1039/c2jm33189f

[93] S. Oh, M.A. Mastro, M.J. Tadjer and J. Kim, *Solar-Blind Metal-Semiconductor-Metal Photodetectors Based on an Exfoliated β-Ga₂O₃ Micro-Flake*, ECS J. Solid State Sci. Technol., 2017, vol. 6, no. 8, pp. Q79–Q83. https://doi.org/10.1149/2.0231708jss

[94] J. Kim, S. Oh, J. Kim, F. Ren and S.J. Pearton, *Quasi-two-dimensional β-gallium oxide solar-blind photodetectors with ultrahigh responsivity*, J. Mater. Chem. C., 2016, vol. 4, pp. 9245–9250. https://doi.org/10.1039/c6tc02467j

[95] M. Zhong, Z. Wei, X. Meng, F. Wu and J. Li, *High-performance single crystalline UV photodetectors of β-Ga₂O₃*, J. Alloys Compd., 2015, vol. 619, pp. 572–575. https://doi.org/10.1016/j.jallcom.2014.09.070

[96] Y.P. Qian, D.Y. Guo, X.L. Chu, H.Z. Shi, W.K. Zhu, K. Wang, X.K. Huang, H. Wang, S.L. Wang, P.G. Li, X.H. Zhang and W.H. Tang, *Mg-doped p-type β-Ga₂O₃ thin film for solar-blind ultraviolet photodetector*, Mater. Lett., 2017, vol. 209, pp. 558–561. https://doi.org/10.1016/j.matlet.2017.08.052

[97] B. Zhao, F. Wang, H. Chen, Y. Wang, M. Jiang, X. Fang and D. Zhao, *Solar-Blind Avalanche Photodetector Based on Single ZnO-Ga₂O₃ Core-Shell Microwire*, Nano Lett., 2015, vol. 15, no. 6, pp. 3988–3993. https://doi.org/10.1021/acs.nanolett.5b00906

[98] S. Ahn, F. Ren, S. Oh, Y. Jung, J. Kim, M.A. Mastro, J.K. Hite, C.R. Eddy and S.J. Pearton,

*Elevated temperature performance of Si-implanted solar-blind β-Ga$_2$O$_3$ photodetectors*, J. Vac. Sci. Technol. B, Nanotechnol. Microelectron. Mater. Process. Meas. Phenom., 2016, vol. 34, no. 4, art. 041207. https://doi.org/10.1116/1.4948361

[99] B.R. Tak, M. Garg, A. Kumar, V. Gupta and R. Singh, *Gamma Irradiation Effect on Performance of β-Ga$_2$O$_3$ Metal-Semiconductor-Metal Solar-Blind Photodetectors for Space Applications*, ECS J. Solid State Sci. Technol., 2019, vol. 8, no. 7, pp. Q3149–Q3153. https://doi.org/10.1149/2.0291907jss

[100] J. Xu, W. Zheng and F. Huang, *Gallium oxide solar-blind ultraviolet photodetectors: a review,* J. Mater. Chem., 2019, vol. 7, pp. 8753–8770. https://doi.org/10.1039/C9TC02055A

[101] D.Y. Lee and T.Y. Tseng, *Forming-free resistive switching behaviors in Cr-embedded Ga$_2$O$_3$ thin film memories*, J. Appl. Phys., 2011, vol. 110, art. 114117. https://doi.org/10.1063/1.3665871

[102] J. Hou, R. Guo, J. Su, Y. Du, Z. Lin, J. Zhang, Y. Hao and J. Chang, *Multilevel oxygen-vacancy conductive filaments in β-Ga$_2$O$_3$ based resistive random access memory*, Phys. Chem. Chem. Phys., 2021, vol. 23, pp. 5975–5983. https://doi.org/10.1039/d0cp06239a

[103] C.H. Pan, T.C. Chang, T.M. Tsai, K.C. Chang, P.H. Chen, S.W. Chang-Chien, M.C. Chen, H.C. Huang, H. Wu, N. Deng, H. Qian and S.M. Sze, *Engineering interface-type resistance switching based on forming current compliance in ITO/Ga$_2$O$_3$:ITO/TiN resistance random access memory: Conduction mechanisms, temperature effects, and electrode influence*, Appl. Phys. Lett, 2016, vol. 109, art. 183509. https://doi.org/10.1063/1.4966181

[104] X.B. Yan, H. Hao, Y.F. Chen, Y.C. Li and W. Banerjee, *Highly transparent bipolar resistive switching memory with In-Ga-Zn-O semiconducting electrode in In-Ga-Zn-O/Ga$_2$O$_3$/In-Ga-Zn-O structure*, Appl. Phys. Lett., 2014, vol. 105, no. 9, art. 093502. https://doi.org/10.1063/1.4894521

[105] Y.S. Zhi, P.G. Li, P.C. Wang, D.Y. Guo, Y.H. An, Z.P. Wu, X.L. Chu, J.Q. Shen, W.H. Tang and C.R. Li, *Reversible transition between bipolar and unipolar resistive switching in Cu$_2$O/Ga$_2$O$_3$ binary oxide stacked layer*, AIP Adv., 2016, vol. 6, no. 1, art. 015215. https://doi.org/10.1063/1.4941061

[106] C.C. Yang, J.Q. Huang, K.Y. Chen, P.H. Chiu, H.T. Vu and Y.K. Su, *Effect of Oxygen Concentration Ratio on a Ga$_2$O$_3$-Based Resistive Random Access Memory*, IEEE Access., 2019, vol. 7, pp. 175186–175191. https://doi.org/10.1109/ACCESS.2019.2948423

[107] K.J. Gan, P.T. Liu, D.B. Ruan, C.C. Hsu, Y.C. Chiu and S.M. Sze, *Effect of Annealing Treatment on Performance of Ga$_2$O$_3$ Conductive-Bridging Random-Access Memory*, J. Electron. Mater., 2020, vol. 49, pp. 6817–6822. https://doi.org/10.1007/s11664-020-08177-9

[108] K. Zheng, X.W. Sun, J.L. Zhao, Y. Wang, H.Y. Yu, H. V. Demir and K.L. Teo, *An indium-free transparent resistive switching random access memory*, IEEE Electron Device Lett., 2011, vol. 32, no. 6, pp. 797–799. https://doi.org/10.1109/LED.2011.2126017

[109] K.J. Gan, P.T. Liu, Y.C. Chiu, D.B. Ruan, T.C. Chien and S.M. Sze, *TAOS based Cu/TiW/IGZO/Ga$_2$O$_3$/Pt bilayer CBRAM for low-power display technology*, Surf. Coatings Technol., 2018, vol. 354, pp. 169–174. https://doi.org/10.1016/j.surfcoat.2018.08.093

[110] X. Shen, L. Zhang, L. Liu, Y. An, Z. Gao and P. Guo, B*ipolar resistive switching of Pt/Ga$_2$O$_{3-x}$/SiC/Pt thin film with ultrahigh OFF/ON resistance ratios*, Nanotechnology, 2020, vol. 31, art. 225206. https://doi.org/10.1088/1361-6528/ab758d

[111] T.F. Weng, M.S. Ho, C. Sivakumar, B. Balraj and P.F. Chung, *VLS growth of pure and Au decorated β-Ga$_2$O$_3$ nanowires for room temperature CO gas sensor and resistive memory applications*, Appl. Surf. Sci., 2020, vol. 533, art. 147476. https://doi.org/10.1016/j.apsusc.2020.147476

[112] C.W. Hsu and L.J. Chou, *Bipolar resistive switching of single gold-in-Ga$_2$O$_3$ nanowire*, Nano Lett., 2012, vol. 12, no. 8, pp. 4247–4253. https://doi.org/10.1021/nl301855u

[113] J.T.H. Tsai, C.H. Hsu, C.Y. Hsu and C.S. Yang, *Rapid synthesis of gallium oxide resistive random access memory by atomic force microscopy local anodic oxidation*, Electron. Lett., 2013, vol. 49, no. 8, pp. 554–555. https://doi.org/10.1049/el.2013.0639

[114] B. Bai, H. Wang, Y. Li, Y. Hao, B. Zhang, B. Wang, Z. Wang, H. Yang, Q. Gao, C. Lü, Q. Zhang and X. Yan, *Charge trapping memory device based on the Ga$_2$O$_3$ films as trapping and blocking layer*, Chinese Phys. B., 2019, vol. 28, no. 10, art. 106802. https://doi.org/10.1088/1674-1056/ab3e62

[115] D. Madadi and A.A. Orouji, *A β-Ga$_2$O$_3$ MESFET to Amend the Carrier Distribution by Using a Tunnel Diode*, IEEE Trans. Device Mater.

Reliab., 2021, vol. 21, no. 1, pp. 26–32. https://doi.org/10.1109/TDMR.2020.3046530

[116] K. Tetzner, O. Hilt, A. Popp, S. Bin Anooz and J. Würfl, *Challenges to overcome breakdown limitations in lateral* β*-Ga$_2$O$_3$ MOSFET devices*, Microelectron. Reliab., 2020, vol. 114, art. 113951. https://doi.org/10.1016/j.microrel.2020.113951

[117] A.J. Green, K.D. Chabak, M. Baldini, N. Moser, R. Gilbert, R.C. Fitch, G. Wagner, Z. Galazka, J. McCandless, A. Crespo, K. Leedy and G.H. Jessen, β*-Ga$_2$O$_3$ MOSFETs for radio frequency operation*, IEEE Electron Device Lett., 2017, vol. 38, no. 6, pp. 790–793. https://doi.org/10.1109/LED.2017.2694805

[118] R. Kotecha, W. Metzger, B. Mather, S. Narumanchi and A. Zakutayev, *Modeling and Analysis of Gallium Oxide Vertical Transistors*, ECS J. Solid State Sci. Technol., 2019, vol. 8, no. 7, pp. Q3202–Q3205. https://doi.org/10.1149/2.0401907jss

[119] Y. Lv, X. Zhou, S. Long, Y. Wang, X. Song, X. Zhou, G. Xu, S. Liang, Z. Feng, S. Cai, X. Fu, A. Pu and M. Liu, *Enhancement-Mode* β*-Ga$_2$O$_3$ Metal-Oxide-Semiconductor Field-Effect Transistor with High Breakdown Voltage over 3000 V Realized by Oxygen Annealing*, Phys. Status Solidi - Rapid Res. Lett., 2020, vol. 14, no. 3, art. 1900586. https://doi.org/10.1002/pssr.201900586

[120] J. Park and S.-M. Hong, *Simulation Study of Enhancement Mode Multi-Gate Vertical Gallium Oxide MOSFETs*, ECS J. Solid State Sci. Technol., 2019, vol. 8, no. 7, pp. Q3116–Q3121. https://doi.org/10.1149/2.0181907jss

[121] J. Kim, M.A. Mastro, M.J. Tadjer and J. Kim, *Heterostructure WSe$_2$-Ga$_2$O$_3$ Junction Field-Effect Transistor for Low-Dimensional High-Power Electronics*, ACS Appl. Mater. Interfaces., 2018, vol. 10, no. 35, pp. 29724–29729. https://doi.org/10.1021/acsami.8b07030

[122] G.T. Dang, T. Kawaharamura, M. Furuta and M.W. Allen, *Mist-CVD Grown Sn-Doped* α*-Ga$_2$O$_3$ MESFETs*, IEEE Trans. Electron Devices., 2015, vol. 62, no. 11, pp. 3640–3644. https://doi.org/10.1109/TED.2015.2477438

[123] J. Kim, M.A. Mastro, M.J. Tadjer and J. Kim, *Quasi-two-dimensional h-BN / β-Ga$_2$O$_3$ heterostructure metal – insulator – semiconductor field-effect transistor,* ACS Appl. Mater. Interfaces, 2017, vol. 9, no. 25, pp. 21322–21327. https://doi.org/10.1021/acsami.7b04374

[124] N. Yadava and R.K. Chauhan, *RF Performance Investigation of* β*-Ga$_2$O$_3$/Graphene and* β*-Ga$_2$O$_3$/Black Phosphorus Heterostructure MOSFETs*, ECS J. Solid State Sci. Technol., 2019, vol. 8, no. 7, pp. Q3058–Q3063. https://doi.org/10.1149/2.0131907jss

[125] Z. Xia, C. Joishi, S. Krishnamoorthy, S. Bajaj, Y. Zhang, M. Brenner, S. Lodha and S. Rajan, *Delta Doped* β*-Ga$_2$O$_3$ Field Effect Transistors with Regrown Ohmic Contacts*, IEEE Electron Device Lett., 2018, vol. 39, no. 4, pp. 568–571. https://doi.org/10.1109/LED.2018.2805785

[126] S. Kim and J. Kim, *Electrical Properties of Thermally Annealed* β*-Ga$_2$O$_3$ Metal-Semiconductor Field-Effect Transistors with Pt/Au Schottky Contacts*, ECS J. Solid State Sci. Technol., 2019, vol. 8, no. 7, pp. Q3122–Q3125. https://doi.org/10.1149/2.0231907jss

[127] K. Matsuzaki, H. Hiramatsu, K. Nomura, H. Yanagi, T. Kamiya, M. Hirano and H. Hosono, *Growth, structure and carrier transport properties of Ga$_2$O$_3$ epitaxial film examined for transparent field-effect transistor*, Thin Solid Films., 2006, vol. 496, no. 1, pp. 37–41. https://doi.org/10.1016/j.tsf.2005.08.187

[128] Y. Zhang, C. Joishi, Z. Xia, M. Brenner, S. Lodha and S. Rajan, *Demonstration of* β*-(Al$_x$Ga$_{1-x}$)$_2$O$_3$/Ga$_2$O$_3$ double heterostructure field effect transistors*, Appl. Phys. Lett., 2018, vol. 112, no. 23, art. 233503. https://doi.org/10.1063/1.5037095

[129] E. Ahmadi, O.S. Koksaldi, X. Zheng, T. Mates, Y. Oshima, U.K. Mishra and J.S. Speck, *Demonstration of* β*-(Al$_x$Ga$_{1-x}$)$_2$O$_3$/β-Ga$_2$O$_3$ modulation doped field-effect transistors with Ge as dopant grown via plasma-assisted molecular beam epitaxy*, Appl. Phys. Express., 2017, vol. 10, no. 7, art. 071101. https://doi.org/10.7567/APEX.10.071101

[130] M. Higashiwaki, K. Sasaki, T. Kamimura, M. Hoi Wong, D. Krishnamurthy, A. Kuramata, T. Masui and S. Yamakoshi, *Depletion-mode Ga$_2$O$_3$ metal-oxide-semiconductor field-effect transistors on* β*-Ga$_2$O$_3$ (010) substrates and temperature dependence of their device characteristics*, Appl. Phys. Lett., 2013, vol. 103, art. 123511. https://doi.org/10.1063/1.4821858

[131] N.A. Moser, J.P. McCandless, A. Crespo, K.D. Leedy, A.J. Green, E.R. Heller, K.D. Chabak, N. Peixoto and G.H. Jessen, *High pulsed current density* β*-Ga$_2$O$_3$ MOSFETs verified by an analytical model corrected for interface charge*, Appl. Phys. Lett., 2017, vol. 110, no. 14, art. 143505. https://doi.org/10.1063/1.4979789

[132] N. Moser, J. McCandless, A. Crespo, K. Leedy, A. Green, A. Neal, S. Mou, E. Ahmadi, J. Speck, K. Chabak, N. Peixoto and G. Jessen, Ge-doped β-*Ga₂O₃* MOSFETs, IEEE Electron Device Lett., 2017, vol. 38, no. 6, pp. 775–778. https://doi.org/10.1109/LED.2017.2697359

[133] N.A. Moser, T. Asel, K.J. Liddy, M. Lindquist, N.C. Miller, S. Mou, A. Neal, D.E. Walker, S. Tetlak, K.D. Leedy, G.H. Jessen, A.J. Green and K.D. Chabak, *Pulsed Power Performance of β-Ga₂O₃ MOSFETs at L-Band*, IEEE Electron Device Lett., 2020, vol. 41, no. 7, pp. 989–992. https://doi.org/10.1109/LED.2020.2993555

[134] J.K. Mun, K. Cho, W. Chang, H.-W. Jung and J. Do, *2.32 kV Breakdown Voltage Lateral β-Ga₂O₃ MOSFETs with Source-Connected Field Plate* , ECS J. Solid State Sci. Technol., 2019, vol. 8, no. 7, pp. Q3079–Q3082. https://doi.org/10.1149/2.0151907jss

[135] K.J. Liddy, A.J. Green, N.S. Hendricks, E.R. Heller, N.A. Moser, K.D. Leedy, A. Popp, M.T. Lindquist, S.E. Tetlak, G. Wagner, K.D. Chabak and G.H. Jessen, *Thin channel β-Ga₂O₃ MOSFETs with self-aligned refractory metal gates*, Appl. Phys. Express., 2019, vol. 12, no.12, art. 126501. https://doi.org/10.7567/1882-0786/ab4d1c

[136] M.H. Wong, K. Goto, Y. Morikawa, A. Kuramata, S. Yamakoshi, H. Murakami, Y. Kumagai and M. Higashiwaki, *All-ion-implanted planar-gate current aperture vertical Ga₂O₃ MOSFETs with Mg-doped blocking layer*, Appl. Phys. Express., 2018, vol. 11, no. 6, art. 064102. https://doi.org/10.7567/APEX.11.064102

[137] M.H. Wong, Y. Nakata, A. Kuramata, S. Yamakoshi and M. Higashiwaki, *Enhancement-mode Ga₂O₃ MOSFETs with Si-ion-implanted source and drain*, Appl. Phys. Express., 2017, vol. 10, no. 4, art. 041101. https://doi.org/10.7567/APEX.10.041101

[138] J. Ma, H.J. Cho, J. Heo, S. Kim and G. Yoo, *Asymmetric Double-Gate β-Ga₂O₃ Nanomembrane Field-Effect Transistor for Energy-Efficient Power Devices*, Adv. Electron. Mater., 2019, vol. 5, no. 6, art. 1800938. https://doi.org/10.1002/aelm.201800938

[139] K.D. Chabak, J.P. McCandless, N.A. Moser, A.J. Green, K. Mahalingam, A. Crespo, N. Hendricks, B.M. Howe, S.E. Tetlak, K. Leedy, R.C. Fitch, D. Wakimoto, K. Sasaki, A. Kuramata and G.H. Jessen, *Recessed-Gate Enhancement-Mode β-Ga₂O₃ MOSFETs*, IEEE Electron Device Lett., 2018, vol. 39, no. 1, pp. 67-70. https://doi.org/10.1109/LED.2017.2779867

[140] K. Sasaki, Q.T. Thieu, D. Wakimoto, Y. Koishikawa, A. Kuramata and S. Yamakoshi, *Depletion-mode vertical Ga₂O₃ trench MOSFETs fabricated using Ga₂O₃ homoepitaxial films grown by halide vapor phase epitaxy*, Appl. Phys. Express., 2017, vol. 10, no. 12, art. 124201. https://doi.org/10.7567/APEX.10.124201

[141] J.F. McGlone, Z. Xia, C. Joishi, S. Lodha, S. Rajan, S. Ringel and A.R. Arehart, *Identification of critical buffer traps in Si δ-doped β-Ga₂O₃ MESFETs*, Appl. Phys. Lett., 2019, vol. 115, art. 153501. https://doi.org/10.1063/1.5118250

[142] A.Y. Polyakov, N.B. Smirnov, I. V. Shchemerov, S. V. Chernykh, S. Oh, S.J. Pearton, F. Ren, A. Kochkova and J. Kim, *Defect States Determining Dynamic Trapping-Detrapping in β-Ga₂O₃ Field-Effect Transistors*, ECS J. Solid State Sci. Technol., 2019, vol. 8, no. 7, pp. Q3013–Q3018. https://doi.org/10.1149/2.0031907jss

[143] M.H. Wong, K. Sasaki, A. Kuramata, S. Yamakoshi and M. Higashiwaki, *Electron channel mobility in silicon-doped Ga₂O₃ MOSFETs with a resistive buffer layer*, Jpn. J. Appl. Phys., 2016, vol. 55, art. 1202B9. https://doi.org/10.7567/JJAP.55.1202B9

[144] S. Luan, L. Dong and R. Jia, *Analysis of the structural, anisotropic elastic and electronic properties of β-Ga₂O₃ with various pressures*, J. Cryst. Growth., 2019, vol. 505, pp. 74–81. https://doi.org/10.1016/j.jcrysgro.2018.09.031

[145] J.E. Stehr, D.M. Hofmann, J. Schörmann, M. Becker, W.M. Chen and I.A. Buyanova, Electron paramagnetic resonance signatures of $Co^{2+}$ and $Cu^{2+}$ in β-Ga₂O₃, Appl. Phys. Lett., 2019, vol. 115, art. 242101. https://doi.org/10.1063/1.5127651

[146] X. Wang, R. Quhe, Y. Zhi, Z. Liu, Y. Huang, X. Dai, Y. Tang, Z. Wu and W. Tang, *The electronic structure and magnetic property of the Mn doped β-Ga₂O₃*, Superlattices Microstruct., 2019, vol. 125, pp. 330–337. https://doi.org/10.1016/j.spmi.2018.12.001

[147] J. Shi, H. Liang, X. Xia, Z. Li, Z. Long, H. Zhang and Y. Liu, *Preparation of high-quality CuGa₂O₄ film via annealing process of Cu/β-Ga₂O₃*, J. Mater. Sci., 2019, vol. 54, pp. 11111–11116. https://doi.org/10.1007/s10853-019-03666-7

[148] Y.S. Hsieh, C.Y. Li, C.M. Lin, N.F. Wang, J. V. Li and M.P. Houng, *Investigation of metal-insulator-semiconductor diode with alpha-Ga₂O₃ insulating layer by liquid phase

*deposition*, Thin Solid Films, 2019, vol. 685, pp. 414–419. https://doi.org/10.1016/j.tsf.2019.06.044

[149] S. Kumar and R. Singh, *Nanofunctional gallium oxide ($Ga_2O_3$) nanowires/nanostructures and their applications in nanodevices*, Phys. Status Solidi - Rapid Res. Lett., 2013, vol. 7, no. 10, pp. 781–792. https://doi.org/10.1002/pssr.201307253

[150] Y.Q. Huang, Y.H. An, Z.P. Wu, D.Y. Guo, Y.S. Zhi, W. Cui, X.L. Zhao and W.H. Tang, *Structural and photoelectrical properties of $Ga_2O_3$/SiC/ $Al_2O_3$ multilayers*, J. Alloys Compd., 2017, vol. 717, pp. 8–13. https://doi.org/10.1016/j.jallcom.2017.05.077

[151] S. Rafique, L. Han, A.T. Neal, S. Mou, J. Boeckl and H. Zhao, *Towards High-Mobility Heteroepitaxial* β-*$Ga_2O_3$ on Sapphire " Dependence on The Substrate Off-Axis Angle*, Phys. Status Solidi Appl. Mater. Sci., 2018, vol. 215, no. 2, art. 1700467. https://doi.org/10.1002/pssa.201700467

[152] H. Sun, C.G. Torres Castanedo, K. Liu, K.H. Li, W. Guo, R. Lin, X. Liu, J. Li and X. Li, *Valence and conduction band offsets of* β-*$Ga_2O_3$/AlN heterojunction*, Appl. Phys. Lett., 2017, vol. 111, art. 162105. https://doi.org/10.1063/1.5003930

[153] C.I.M. Rodríguez, M.Á.L. Álvarez, J. de J.F. Rivera, G.G.C. Arízaga and C.R. Michel, α-*$Ga_2O_3$ as a Photocatalyst in the Degradation of Malachite Green*, ECS J. Solid State Sci. Technol., 2019, vol. 8, no. 7, pp. Q3180–Q3186. https://doi.org/10.1149/2.0351907jss

[154] M. Peres, A.J.S. Fernandes, F.J. Oliveira, L.C. Alves, E. Alves, T.S. Monteiro, S. Cardoso, M. Alonso-Orts, E. Nogales, B. Méndez, E.G. Víllora, K. Shimamura and K. Lorenz, *Micro-Opto-Electro-Mechanical Device Based on Flexible* β-*$Ga_2O_3$ Micro-Lamellas*, ECS J. Solid State Sci. Technol., 2019, vol. 8, no. 7, pp. Q3235–Q3241. https://doi.org/10.1149/2.0441907jss